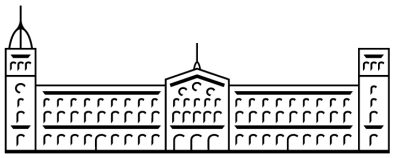

Bachelor Thesis

DEGREE IN MATHEMATICS

Faculty of Mathematics
University of Barcelona

Study and simulation of the Planar and Circular Restricted Three-Body Problem

---

Author: Albert Solà Vilalta

Director:	Dr. Antoni Benseny Ardiaca
Realized in:	Department of Applied Mathematics and Analysis

Barcelona, July 24, 2015

Abstract

We study the Planar and Circular Restricted Three-Body Problem, as an idealization of the Three-Body Problem. We follow a dynamical systems approach. Once the main characteristics of the problem have been described, we try to explore a little bit the chaos of the system. Without pretending to be systematic, we focus on final evolutions. In particular, the parabolic final evolutions are used to show evidence of chaos, as they correspond to the invariant manifolds of the periodic orbit at infinity, which intersect non-tangentially in a certain Poincaré section, giving rise to transversal homoclinic points of the associated Poincaré map.

Furthermore, we try to outline some differences between the integrable Kepler Problem and the non-integrable Planar and Circular Restricted Three-Body Problem, which can be explained by the splitting of the two previously mentioned invariant manifolds. The use of numerical methods has been fundamental for the realization of this work.

Acknowledgements

During the realitzation of this work, it has been crucial the tuition and constant help of Dr. Antoni Benseny, the director of this thesis. My most sincere words of thanks for guiding me through the Three-Body problem. At a similar level, the unconditional support of my family and friends has definitely had a positive effect on this work, specially in the difficult moments.

Contents

1 Introduction

The project

One of the subjects of the Bachelor in Mathematics I found particularly interesting was Differential Equations, maybe because it involved many other parts of mathematics, such as Analysis, Topology, Geometry or Numerical Mathematics. That is mainly why I decided to look for a topic somehow related to it. Furthermore, at the moment of the choice I had the impression that a more applied mathematics oriented Bachelor's thesis would be more interesting and challenging. I now think that both options are equally valid, but I do not regret my choice.

After commenting my interests with Dr. Antoni Benseny, the Three-Body Problem came out as a possible topic. Its simple physical enunciate combined with its difficult treatment, that required the use of a wide range of mathematics, some of them already studied in the Bachelor, definitely attracted me. Due to the great difficulties that surround the general Three-Body Problem, we decide to focus on the Planar and Circular Restricted Three-Body Problem, as a first approximation to the general Three-Body Problem when one of the masses is much smaller than the others.

The main objective of this thesis was to introduce myself in the Planar and Circular Restricted Three-Body Problem, for both its own interest and the fact of dealing with a complicated dynamical system. In that sense, as I did not know much about the particular topic beforehand, there was not an initial objective of studying an specific aspect of the problem, but this should be chosen during the realization of the thesis.

It is important to stress that during the realization of this thesis I took part in the optional subject Dynamical Systems, which definitely has had an influence on this work, specially in the treatment of chaos done in the last section.

Structure of the report

The report of this thesis is structured in three chapters, but the Planar and Circular Restricted Three-Body Problem, the main topic of the thesis, is only considered in the last and most extensive chapter.

The first chapter is an introduction to the general n-Body Problem, where the problem is posed and the main basic results are stated without proof. Special emphasis is given to the first integrals. It has been included in order to emphasize the generality of some results.

The second chapter takes a look at the Two-Body Problem. Apart of being interesting by itself, it plays a crucial role in the Restricted Three-Body Problem, not necessarily Planar and Circular, as the primaries behave as in the Two-Body Problem. Furthermore, the treatment done of Kepler's Problem is also crucial, as the Planar and Circular Restricted Three-Body Problem can be understood as a

perturbation of it for small values of the mass parameter m. We will follow this point of view in some parts of the next chapter.

The third chapter deals with the Planar and Circular Restricted Three-Body Problem itself. It could be divided into two main parts. The first three sections, in which the equations of motion are derived in several coordinate frames and the skeleton of the system is described in detail. The last section concludes with a try to approach the chaos of the system in a particular aspect of the problem. Numerical evidence of chaos is provided. In order to do it, orbits of the third body have been simulated, with emphasis on the parabolic final evolution for positive or negative time. Due to the increase of difficulty of this last part, the presentation is no longer systematic and many advanced results have been used from other sources.

2 Systems of n particles

2.1 General results

To begin with, we will study some basic features of systems of n particles. It is a much more general setting than the required for the study of both the Two-Body Problem and the Planar and Circular Restricted Three-Body Problem. However, some of the results obtained are relevant for the two problems mentioned above, so it is convenient to consider it separately. We advance here that the restricted assumption makes these results not valid for the Planar and Circular Restricted Three-Body Problem, as it will be discussed later. This section is a summary of results, not a proper development of the topic. It is mainly based on [9], where the details are made more explicit.

Consider a system of n particles subjected to both internal and external forces (forces done on a particle of the system by another particle of the system or by an external agent). Fix an inertial reference frame $\{O; \boldsymbol{x}, \boldsymbol{y}, \boldsymbol{z}\}$ on $\mathbb{R}^3$.

Let $\boldsymbol{r}_i = \boldsymbol{r}_i(t)$ be the position vector of the i-th particle with respect to the reference frame at time t, m_i its mass, $\boldsymbol{F}_{ji}(t)$ the force done by particle j to particle i at time t and $\boldsymbol{F}_i(t)$ the external force done to particle i at time t. According to Newton's second law, the vectorial equations of motion for the particles are

$$m_i \ddot{\boldsymbol{r}}_i = \boldsymbol{F}_i + \sum_{j \neq i}^{n} \boldsymbol{F}_{ji} \qquad 1 \leq i \leq n \tag{2.1}$$

where $\ddot{\boldsymbol{r}}_i := \frac{d^2 \boldsymbol{r}_i}{dt^2}$. The main results of the section are variational results, from which the corresponding conservation laws are easily deduced. We focus on the conservation of the total linear momentum, the total angular momentum and the energy.

Def 2.1. *The linear momentum $\boldsymbol{p}$ of a particle of mass m is*

$$\boldsymbol{p}(t) := m\boldsymbol{v}(t) \tag{2.2}$$

where $\boldsymbol{v} = \frac{d\boldsymbol{r}}{dt}$ is its velocity vector. Let $\boldsymbol{p}_i$ be the linear momentum of the i-th particle. The total linear momentum $\boldsymbol{P}$ of the system is

$$\boldsymbol{P}(t) := \sum_{i=1}^{n} \boldsymbol{p}_i(t) \tag{2.3}$$

Def 2.2. *The angular momentum $\boldsymbol{L}$ of a particle of mass m is*

$$\boldsymbol{L}(t) := \boldsymbol{r}(t) \times \boldsymbol{p}(t) \tag{2.4}$$

where $\boldsymbol{r}$ is its position vector and $\boldsymbol{p}$ its linear momentum. Let $\boldsymbol{L}_i$ be the angular momentum of the i-th particle. The total angular momentum $\boldsymbol{L}$ of the system is

$$\boldsymbol{L} := \sum_{i=1}^{n} \boldsymbol{L}_i = \sum_{i=1}^{n} \boldsymbol{r}_i \times \boldsymbol{p}_i \tag{2.5}$$

Theorem 2.1.

$$\frac{d\boldsymbol{P}}{dt} = \sum_{i=1}^{n} \boldsymbol{F}_i =: \boldsymbol{F}$$

where $\boldsymbol{F}$ denotes the sum of all the exterior forces acting on the system.

Corollary 2.1. *(Conservation of linear momentum) Under the abscence of external forces, the total linear momentum remains constant.* □

We investigate now the motion of the center of mass.

Def 2.3. *The center of mass $\boldsymbol{R}$ of a system of n particles is*

$$\boldsymbol{R} = \frac{1}{M}\sum_{i=1}^{n} m_i \boldsymbol{r}_i \qquad \text{where } M := \sum_{i=1}^{n} m_i \tag{2.6}$$

It is also called the barycenter of the system. The velocity $\boldsymbol{V}$ of the center of mass is

$$\boldsymbol{V} := \frac{d\boldsymbol{R}}{dt} = \frac{1}{M}\sum_{i=1}^{n} \boldsymbol{p}_i \tag{2.7}$$

Observe that, deriving (2.6) twice with respect to t,

$$M\frac{d\boldsymbol{R}}{dt} = \sum_{i=1}^{n} m_i \frac{d\boldsymbol{r}_i}{dt} = \sum_{i=1}^{n} \boldsymbol{p}_i = \boldsymbol{P}; \qquad M\frac{d^2\boldsymbol{R}}{dt^2} = \frac{d\boldsymbol{P}}{dt} = \boldsymbol{F} \tag{2.8}$$

where we have used Theorem 2.1. So, the center of mass of a system of n particles moves as a single particle of mass M under the effects of a force equal to $\boldsymbol{F}$. For our next development, it is useful to notice the following corollary:

Corollary 2.2. *If the total exterior force $\boldsymbol{F}$ is zero, the center of mass remains stationary or moves on a line with constant velocity.* □

Theorem 2.2.

$$\frac{d\boldsymbol{L}}{dt} = \sum_{i=1}^{n} \boldsymbol{r}_i \times \boldsymbol{F}_i =: \boldsymbol{K}$$

where $\boldsymbol{K}$ is the exterior total momentum.

Corollary 2.3. *(Conservation of angular momentum) Under the abscence of external forces, the total angular momentum remains constant.* □

To state the conservation of energy, we need to introduce conservative forces.

Def 2.4. *A force $\boldsymbol{F}$ is conservative if there exists a function $U : \Omega \subseteq \mathbb{R}^3 \longrightarrow \mathbb{R}$ such that*

$$\boldsymbol{F} = -\nabla U = -\left(\frac{\partial U}{\partial x}, \frac{\partial U}{\partial y}, \frac{\partial U}{\partial z}\right) \tag{2.9}$$

where Ω is the positions domain of definition of the force F. The function U is the potential energy of $\boldsymbol{F}$.

Def 2.5. *The potential energy U of the system is the sum of all the potential energies associated to conservative forces acting on particles of the system.*

Def 2.6. *The kinetic energy T of a particle of mass m is*

$$T := \frac{1}{2}mv^2 \tag{2.10}$$

where v denotes the magnitude of its velocity. Let T_i be the kinetic energy of the i-th particle. The kinetic energy T of the system is

$$T := \sum_{i=1}^{n} T_i = \frac{1}{2}\sum_{i=1}^{n} m_i v_i^2 \tag{2.11}$$

Theorem 2.3. *(Conservation of energy) If all the forces acting on the system are conservative, then the total energy E*

$$E := T + U \tag{2.12}$$

is conserved, where T and U denote the kinetic and the potential energies of the system.

2.2 The n-Body Problem

The n-Body Problem consists on the study of the motion of n punctual particles, in the space $\mathbb{R}^3$, which are only subjected to their mutual gravitational forces. There is no known general solution for the case $n \geq 3$, but some basic features, which follow from the previous section, can be said in general. We shall describe them here. The equations of motion for the n bodies are obtained from Newton's second law and Newton's law of universal gravitation, namely

$$m_i \ddot{\boldsymbol{r}}_i = \sum_{j \neq i} -G\frac{m_i m_j}{r_{ji}^3}\boldsymbol{r}_{ji} \qquad\qquad 1 \leq i \leq n \tag{2.13}$$

where $\boldsymbol{r}_i$ is the position vector of the i-th particle, m_i its mass, G the gravitational constant and r_{ji} the modulus of $\boldsymbol{r}_{ji} := \boldsymbol{r}_i - \boldsymbol{r}_j$.

First of all, note that there are no external forces acting on the system. Thus, we can conclude that the linear momentum of the system $\boldsymbol{P}$, the velocity of the center of mass $\boldsymbol{V}$ and the angular momentum of the system $\boldsymbol{L}$ are constants of motion (Corollaries 2.1, 2.2 and 2.3).

Secondly the gravitational force $\boldsymbol{F}_{ji}$ done by particle j to particle i

$$\boldsymbol{F}_{ji} = -G\frac{m_i m_j}{r_{ji}^3}\boldsymbol{r}_{ji} \tag{2.14}$$

is a conservative force, as the function

$$U_{ji} := -G\frac{m_i m_j}{r_{ji}} \tag{2.15}$$

satisfies

$$\boldsymbol{F}_{ji} = -\nabla_j U_{ji} = -\left(\frac{\partial U_{ji}}{\partial x_j}, \frac{\partial U_{ji}}{\partial y_j}, \frac{\partial U_{ji}}{\partial z_j}\right)$$

Thus, the energy is conserved (Theorem 2.3).

Def 2.7. *Let $f : \Omega \subseteq \mathbb{R}^n \longrightarrow \mathbb{R}^n$, $\dot{\boldsymbol{x}} = \boldsymbol{f}(\boldsymbol{x})$ be an autonomous system of differential equations. A first integral of the system is a non-constant function $H : \Omega \subset \mathbb{R}^n \longrightarrow \mathbb{R}$, which is constant along the solutions of the equation. Namely, if $\varphi : I \subset \mathbb{R} \longrightarrow \mathbb{R}^n$ is a solution of the differential equation, then*

$$H(\varphi(t)) = H(\varphi(0)) \qquad \forall t \in I$$

Summarizing, we have found the ten classical first integrals of the n-Body Problem in $\mathbb{R}^3$: three corresponding to the linear momentum of the system $\boldsymbol{P}$; three corresponding to the constant velocity of the center of mass $\dot{\boldsymbol{R}} = \boldsymbol{V}$; three corresponding to the angular momentum of the system $\boldsymbol{L}$; one corresponding to the total energy E.

3 The Two-Body Problem

3.1 Equations of motion. First consequences

The Two-Body Problem, as the name suggests, is the n-Body Problem assuming $n = 2$. Consider two punctual particles with masses m_1, m_2. They will be referred as the first and the second body. We will follow a Newtonian mechanics approach, which will be mainly based on [2] and [9].

Fix an inertial reference frame $\{O; \boldsymbol{x}, \boldsymbol{y}, \boldsymbol{z}\}$ and consider the position vectors $\boldsymbol{r}_1, \boldsymbol{r}_2$ of the bodies with respect to it. Following from (2.13), the equations of motion for the two bodies are

$$m_1\ddot{\boldsymbol{r}}_1 = -\frac{Gm_1m_2}{r_{21}^3}\boldsymbol{r}_{21}; \qquad m_2\ddot{\boldsymbol{r}}_2 = -\frac{Gm_1m_2}{r_{12}^3}\boldsymbol{r}_{12} \tag{3.1}$$

The main objective of this section is to describe and try to solve (3.1). As the center of mass moves at constant velocity, we introduce the following change of variables

$$\boldsymbol{r} = \boldsymbol{r}_{12} = \boldsymbol{r}_2 - \boldsymbol{r}_1; \qquad \boldsymbol{R} = \frac{m_1\boldsymbol{r}_1 + m_2\boldsymbol{r}_2}{m_1 + m_2} \tag{3.2}$$

where $\boldsymbol{R}$ is the center of mass of the system and $\boldsymbol{r}$ is the relative position vector, with origin at the first body. These coordinates are called barycentric coordinates. Straightforward calculations give the inverse change

$$\boldsymbol{r}_1 = \boldsymbol{R} - \frac{m_2}{m_1 + m_2}\boldsymbol{r}; \qquad \boldsymbol{r}_2 = \boldsymbol{R} + \frac{m_1}{m_1 + m_2}\boldsymbol{r} \tag{3.3}$$

The equations of motion (3.1) in barycentric coordinates are

$$\ddot{\boldsymbol{R}} = \frac{1}{m_1 + m_2}(m_1\ddot{\boldsymbol{r}}_1 + m_2\ddot{\boldsymbol{r}}_2) = 0; \qquad \ddot{\boldsymbol{r}} = \ddot{\boldsymbol{r}}_2 - \ddot{\boldsymbol{r}}_1 = -\frac{m_1 + m_2}{m_1m_2}\frac{Gm_1m_2}{r^3}\boldsymbol{r} \tag{3.4}$$

this is

$$\boldsymbol{R} = V_0t + R_0; \qquad \mu\ddot{\boldsymbol{r}} = -\frac{Gm_1m_2}{r^3}\boldsymbol{r} = -\frac{G\mu M}{r^3}\boldsymbol{r} \tag{3.5}$$

where $\mu := \frac{m_1m_2}{m_1+m_2}$ is the reduced mass and $M := m_1+m_2$ is the total mass. Observe that the motion of the center of mass $\boldsymbol{R}$ is already determined: $\boldsymbol{R}$ moves at constant velocity along a straight line. In fact, we already knew it for a system of n-particles (Corollary 2.2). Also, the equation for $\boldsymbol{r}$ is familiar, as it is the same equation as the one for motion of a particle of mass μ under the gravitational field of a particle of mass M, this is, Kepler's problem.

We would like to take advantage of the first integrals found for the general n-Body Problem in the case $n = 2$. First of all, observe that if we situate the origin at the center of mass $\boldsymbol{R}$, the resulting reference frame is inertial, as the center of mass moves at constant velocity with respect to the original reference frame. Thus, Newton's laws continue to hold. It corresponds to the change of coordinates (3.2).

The second important result that can be rapidly obtained is that in a reference frame where the origin is located at one of the bodies or at the center of mass, the motion of the two bodies takes place in a plane.

Consider the case where the origin is located at one of the bodies, say the first body. Then,

$$\boldsymbol{L} = m_1(\boldsymbol{r}_1 \times \boldsymbol{v}_1) + m_2(\boldsymbol{r}_2 \times \boldsymbol{v}_2) = m_2(\boldsymbol{r}_2 \times \boldsymbol{v}_2) \tag{3.6}$$

as $\boldsymbol{r}_1 = 0$ (and, in fact, also $\boldsymbol{v}_1 = 0$) due to the choice of the origin. According to the conservation of angular momentum, $\boldsymbol{L}$ remains constant, and thus the second body is always located in the plane which is orthogonal to $\boldsymbol{L}$, this is, the plane generated by $\boldsymbol{r}_2(0), \boldsymbol{v}_2(0)$. Note also that the first body is also in this plane, as $\boldsymbol{r}_2$ has its origin in the first body (the origin of the system).

Consider the case where the origin is at the center of mass. The angular momentum can be expressed in terms of barycentric coordinates (3.2) as

$$\boldsymbol{L} = m_1(\boldsymbol{r}_1 \times \boldsymbol{v}_1) + m_2(\boldsymbol{r}_2 \times \boldsymbol{v}_2) = (m_1 + m_2)(\boldsymbol{R} \times \boldsymbol{V}) + \frac{m_1 m_2}{m_1 + m_2}(\boldsymbol{r} \times \boldsymbol{v}) \tag{3.7}$$

where $\boldsymbol{V} := \frac{d\boldsymbol{R}}{dt}$ and $\boldsymbol{v} := \frac{d\boldsymbol{r}}{dt}$ are the respective velocities. As the origin is at the center of mass, $\boldsymbol{R} = 0$ (and, in fact, also $\boldsymbol{V} = 0$). Thus the first term vanishes. According to the conservation of angular momentum

$$\boldsymbol{L} = \frac{m_1 m_2}{m_1 + m_2}(\boldsymbol{r} \times \boldsymbol{v}) = \text{ ctant} \tag{3.8}$$

So the relative position vector $\boldsymbol{r}$ is restricted to the plane which is orthogonal to $\boldsymbol{L}$. As $\boldsymbol{R} = \boldsymbol{R}_0 = 0$, due to (3.2), $\boldsymbol{r}_1, \boldsymbol{r}_2$ are parallel to $\boldsymbol{r}$. For the same reason, $\dot{\boldsymbol{r}}_1, \dot{\boldsymbol{r}}_2$ are parallel to $\dot{\boldsymbol{r}}$, so the motion of the two bodies takes place in the plane orthogonal to $\boldsymbol{L}$.

3.2 Motion under central fields

To complete the study of the Two-Body Problem remains to solve the second equation of (3.5), which reduces to

$$\ddot{\boldsymbol{r}} = -\frac{GM}{r^3}\boldsymbol{r} \tag{3.9}$$

In this section, we study the motion under a general central field of the plane, as the field involved in the previous equation is of this type. The specific treatment of (3.9) is done in the next section.

Def 3.1. *A field $\boldsymbol{f} : \Omega \subseteq \mathbb{R}^2 \longrightarrow \mathbb{R}^2$ of the plane is central with center at 0 if all the vectors of the field lie on rays through 0 and the magnitude of the field at a point depends only on the distance from the point to the center of the field.*

An interesting feature of central fields is that central fields are conservative, as we shall see on Theorem 3.3. Thus, we will describe the main characteristics of conservative fields. Analogously to conservative forces, conservative fields are defined as follows

Def 3.2. *A field* $\boldsymbol{f} : \Omega \subseteq \mathbb{R}^2 \longrightarrow \mathbb{R}^2$ *is conservative if there exists a function* $U : \Omega \subseteq \mathbb{R}^2 \longrightarrow \mathbb{R}$ *such that*

$$\boldsymbol{f} = -\nabla U = -\left(\frac{\partial U}{\partial x}, \frac{\partial U}{\partial y}\right) \tag{3.10}$$

The function U *is the potential energy of the field.*

We will proof here the conservation of energy under conservative fields. We omitted previously the corresponding proof for systems of n particles (Theorem 2.3), but its proof could follow in a similar manner.

Theorem 3.1. *The total energy* E *per unit mass of a conservative field*

$$E := \frac{1}{2}|\dot{\boldsymbol{r}}|^2 + U(r) = \frac{1}{2}(\dot{x}^2 + \dot{y}^2) + U(x, y) \tag{3.11}$$

is conserved.

Proof.

$$\frac{dE}{dt} = \dot{x}\ddot{x} + \dot{y}\ddot{y} + \frac{\partial U}{\partial x}\dot{x} + \frac{\partial U}{\partial y}\dot{y} = 0$$

due to (3.10). □

Def 3.3. *The line integral of a vector field* $\boldsymbol{f}$ *along a curve* γ *with extremes* $\alpha, \beta \in \mathbb{R}^2$ *is the integral of the field along the curve, namely*

$$\int_\gamma \boldsymbol{f} \cdot ds := \int_a^b \boldsymbol{f}(\boldsymbol{\gamma}(t)) \cdot \boldsymbol{\gamma}'(t)dt \tag{3.12}$$

where $\boldsymbol{\gamma} : [a, b] \in \mathbb{R} \longrightarrow \mathbb{R}^2$ *is a parametritzation of the curve* γ*, with* $\boldsymbol{\gamma}(a) = \alpha, \boldsymbol{\gamma}(b) = \beta$ *and* $\cdot$ *denotes the scalar product.*

Theorem 3.2. *A vector field* $\boldsymbol{f}$ *is conservative if, and only if, its line integral* $\int_\gamma \boldsymbol{f} \cdot ds$ *along any curve* γ *with extremes* α, β *depends only on the extremes* α, β*, and not on the shape of the curve.*

A proof of this classical result can be seen in many books, for instance see [2].

Theorem 3.3. *Every central field is conservative, and its potential energy depends only on the distance to the center of the field,* $U = U(\boldsymbol{r}) = U(r)$

Proof. As the central field $\boldsymbol{f}$ lies on rays through 0 and the magnitude f of the vector field depends only on the distance to 0 (the center of the field), we can write

$$\boldsymbol{f}(\boldsymbol{r}) = \phi(r)\frac{\boldsymbol{r}}{r} \tag{3.13}$$

where $\phi = \phi(r)$ is a scalar function depending only on r. According to Theorem 3.2, it is enough to check that the line integral of $\boldsymbol{f}$ along any curve γ with extremes

$\alpha, \beta \in \mathbb{R}^2$ does not depend on the shape of the curve. Let γ be a curve with extremes α, β. Then,

$$\int_\gamma \boldsymbol{f} \cdot ds := \int_a^b \boldsymbol{f}(\boldsymbol{\gamma}(t)) \cdot \boldsymbol{\gamma}'(t)dt = \int_a^b \left(\frac{\phi(|\boldsymbol{\gamma}(t)|)}{|\boldsymbol{\gamma}(t)|} \right) \boldsymbol{\gamma}(t) \cdot \boldsymbol{\gamma}'(t)dt = \int_{|\boldsymbol{\gamma}(a)|}^{|\boldsymbol{\gamma}(b)|} \phi(r)dr \tag{3.14}$$

where we introduced the change of variables $r := |\boldsymbol{\gamma}(t)|, dr = \frac{1}{|\boldsymbol{\gamma}(t)|}\boldsymbol{\gamma}(t) \cdot \boldsymbol{\gamma}'(t)dt$. This integral depends only on the modulus of the endpoints $\gamma(a) = \alpha, \gamma(b) = \beta$ of γ, and thus it is independent of the shape of γ. □

Theorem 3.4. *Under a central field, the angular momentum per unit mass* $\boldsymbol{L} := \boldsymbol{r} \times \dot{\boldsymbol{r}}$ *is conserved.*

Proof.

$$\frac{d\boldsymbol{L}}{dt} = \dot{\boldsymbol{r}} \times \dot{\boldsymbol{r}} + \boldsymbol{r} \times \ddot{\boldsymbol{r}} = \frac{\phi(r)}{r} \boldsymbol{r} \times \boldsymbol{r} = 0$$

□

Consider polar coordinates on the plane with origin at the center of the field 0. For every point, with polar coordinates (r, φ), consider two vectors $\boldsymbol{e}_r, \boldsymbol{e}_\varphi$, with origin at the point corresponding to (r, φ), defined by

$$\boldsymbol{e}_r := \frac{1}{r}\boldsymbol{r} = (\cos\varphi(t), \sin\varphi(t)); \qquad \boldsymbol{e}_\varphi := (-\sin\varphi(t), \cos\varphi(t)) \tag{3.15}$$

Note that for every point with coordinates (r, φ), $(\boldsymbol{e}_r, \boldsymbol{e}_\varphi)$ is a base of the tangent space at (r, φ).

Lema 3.1.

$$\dot{\boldsymbol{r}} = \dot{r}\boldsymbol{e}_r + r\dot{\varphi}\boldsymbol{e}_\varphi \tag{3.16}$$

Proof. As $\boldsymbol{r}(t) = (r(t)\cos\varphi(t), r\sin\varphi(t))$,

$$\dot{\boldsymbol{r}} = (\dot{r}\cos\varphi - r\dot{\varphi}\sin\varphi, \dot{r}\sin\varphi + r\dot{\varphi}\cos\varphi) = \dot{r}\boldsymbol{e}_r + r\dot{\varphi}\boldsymbol{e}_\varphi$$

□

The angular momentum per unit mass is then

$$\boldsymbol{L} = (\boldsymbol{r} \times \dot{\boldsymbol{r}}) = r[\boldsymbol{e}_r \times (\dot{r}\boldsymbol{e}_r + r\dot{\varphi}\boldsymbol{e}_\varphi)] = r^2\dot{\varphi}(\boldsymbol{e}_r \times \boldsymbol{e}_\varphi); \qquad L = r^2\dot{\varphi} \tag{3.17}$$

Theorem 3.5. *In a central field, the distance* r *of a point of unitary mass from the center of the field varies in the same way as* r *varies in the one-dimensional problem with potential energy per unit mass*

$$U_{ef}(r) = U(r) + \frac{L^2}{2r^2} \tag{3.18}$$

Proof. First of all, note that deriving from (3.15), we get

$$\dot{\boldsymbol{e}}_r = (-\dot{\varphi}\sin\varphi, \dot{\varphi}\cos\varphi) = \dot{\varphi}\boldsymbol{e}_\varphi; \qquad \dot{\boldsymbol{e}}_\varphi = (-\varphi\cos\varphi, -\dot{\varphi}\sin\varphi) = -\dot{\varphi}\boldsymbol{e}_r \tag{3.19}$$

Deriving from (3.16), we get

$$\ddot{\boldsymbol{r}} = \ddot{r}\boldsymbol{e}_r + \dot{r}\dot{\boldsymbol{e}}_r + \dot{r}\dot{\varphi}\boldsymbol{e}_\varphi + r\ddot{\varphi}\boldsymbol{e}_\varphi + r\dot{\varphi}\dot{\boldsymbol{e}}_\varphi = (\ddot{r} - r\dot{\varphi}^2)\boldsymbol{e}_r + (2\dot{r}\dot{\varphi} + r\ddot{\varphi})\boldsymbol{e}_\varphi \tag{3.20}$$

As the field is central,

$$\nabla U(r) = \left(\frac{\partial U}{\partial x}(r), \frac{\partial U}{\partial y}(r)\right) = \frac{\partial U}{\partial r}\frac{1}{r}(x, y) = \frac{\partial U}{\partial r}\boldsymbol{e}_r \tag{3.21}$$

From (3.20) and (3.21) we get the equations of motion in polar coordinates

$$\ddot{r} - r\dot{\varphi}^2 = -\frac{\partial U}{\partial r}; \qquad 2\dot{r}\dot{\varphi} + r\ddot{\varphi} = 0 \tag{3.22}$$

But, as $L = r^2\dot{\varphi}$

$$\ddot{r} = -\frac{\partial U}{\partial r} + \frac{L^2}{r^3} = -\frac{\partial U_{ef}}{\partial r} \qquad \text{where} \quad U_{ef}(r) := U(r) + \frac{L^2}{2r^2} \tag{3.23}$$

□

Remark 3.1. *It follows from Theorem 3.1 that the energy per unit mass is conserved in both the central field problem and the one-dimensional problem for r. Furthermore, both values of energy coincide, as the energy per unit mass corresponding to the central field problem is, according to* (3.11)

$$E := \frac{1}{2}(\dot{x}^2 + \dot{y}^2) + U(r) =$$

$$= \frac{1}{2}[\dot{r}^2\cos^2\varphi + r^2\dot{\varphi}^2\sin^2\varphi - 2r\dot{r}\dot{\varphi}\sin\varphi\cos\varphi + \dot{r}^2\sin^2\varphi + r^2\dot{\varphi}^2\cos^2\varphi + 2r\dot{r}\dot{\varphi}\sin\varphi\cos\varphi]$$

$$+U(r) = \frac{1}{2}\dot{r}^2 + \frac{1}{2}r^2\dot{\varphi}^2 + U(r) = \frac{1}{2}\dot{r}^2 + \frac{L^2}{2r^2} + U(r) = \frac{1}{2}\dot{r}^2 + U_{ef}(r) \tag{3.24}$$

We are now ready to describe the motion of a particle under a central field. First of all, we should solve the equations of motion. The solution will not be explicit, as it will depend on some integrals.

From (3.24), as E remains constant

$$\dot{r} = \frac{dr}{dt} = \sqrt{2(E - U_{ef}(r))}; \qquad \int_{t_0}^{t} \frac{\dot{r}(\tau)}{\sqrt{2(E - U_{ef}(r))}} d\tau = t - t_0 \tag{3.25}$$

After the change of variables $\rho = r(\tau)$, we get

$$\int_{r_0}^{r} \frac{d\rho}{\sqrt{2(E - U_{ef}(\rho))}} = t - t_0 \tag{3.26}$$

Similarly for φ, from (3.17)

$$\dot{\varphi} = \frac{L}{r^2}; \qquad \varphi(t) = \varphi(t_0) + L\int_{t_0}^{t} \frac{1}{r(\tau)^2} d\tau \tag{3.27}$$

Equations (3.26) and (3.27) solve, up to the computation of one integral, the equations of motion for r and φ. Another interesting feature is to characterize the trajectory, again up to the calculation of an integral. To that end, from (3.17), consider

$$\frac{L}{r^2} = \frac{d}{dt}[\varphi(r(t))] = \frac{d\varphi}{dr}(r(t))\dot{r}(t) = \frac{d\varphi}{dr}(r)\sqrt{2(E-U_{ef})}; \qquad \frac{d\varphi}{dr} = \frac{L}{r^2\sqrt{2(E-U_{ef})}} \tag{3.28}$$

Integrating both sides with respect to r

$$\varphi(r) = \varphi(r_0) + L\int_{r_0}^{r} \frac{1}{\rho^2\sqrt{2(E-U_{ef}(\rho))}} d\rho \tag{3.29}$$

3.3 Kepler's problem

We would like to solve equation (3.5) for the relative position vector $\boldsymbol{r}$ in the Two-Body Problem, namely

$$\ddot{\boldsymbol{r}} = -\frac{GM}{r^3}\boldsymbol{r} \tag{3.30}$$

Observe that it is a central field. Thus, equations (3.26) and (3.27) give a solution for the problem, up to the computation of some integrals. It is particularly interesting the equation for the trajectory (3.29), which can be solved explicitly and allows to describe the type of orbits the particle follows. In this case, the potential energy and the effective potential energy (both per unit mass) are given by

$$U(r) = -\frac{k}{r}; \qquad U_{ef}(r) = -\frac{k}{r} + \frac{L^2}{2r^2} \qquad \text{where } k = GM \tag{3.31}$$

Following from (3.29), introducing the change of variables $\tilde{\rho} = \frac{1}{\rho}$

$$\varphi(r) = \varphi(r_0) + L\int_{r_0}^{r} \frac{1}{\rho^2\sqrt{2(E-U_{ef}(\rho))}} d\rho = \varphi(r_0) - \int_{1/r_0}^{1/r} \frac{d\tilde{\rho}}{\sqrt{\frac{2E}{L^2} + \frac{2k}{L^2}\tilde{\rho} - \tilde{\rho}^2}}$$

where the last integral is of the form

$$\int \frac{dx}{\sqrt{A + 2Bx - x^2}} = \int \frac{dx}{\sqrt{(B^2+A) - (x-B)^2}} = \frac{1}{\sqrt{B^2+A}} \int \frac{dx}{\sqrt{1 - \left(\frac{x-B}{\sqrt{B^2+A}}\right)^2}}$$

with $A = \frac{2E}{L^2}, B = \frac{k}{L^2}$. After the change of variables $y = \frac{x-B}{\sqrt{B^2+A}}$, it turns out to be

$$\int \frac{dy}{\sqrt{1-y^2}} = -\arccos(y) = -\arccos\left(\frac{x-B}{\sqrt{B^2+A}}\right) \tag{3.32}$$

Eccentricity	Energy	Orbit
$\epsilon < 0$	$E < E_{\min}$	Not possible
$\epsilon = 0$	$E = E_{\min}$	Circle
$0 < \epsilon < 1$	$E_{\min} < E < 0$	Ellipse
$\epsilon = 1$	$E = 0$	Parabola
$\epsilon > 1$	$E > 0$	Hyperbola

Figure 1: Type of orbit depending on the eccentricity ϵ or energy E

So, undoing the changes, the solution is

$$\varphi(r) = \arccos\left(\frac{\frac{L}{r} - \frac{k}{L}}{\sqrt{2E + \frac{k^2}{L^2}}}\right) \tag{3.33}$$

where we have chosen the constant of integration such that the term $\varphi(r_0)$ vanishes. Introducing the terms

$$\epsilon := \sqrt{1 + \frac{2EL^2}{k^2}}; \qquad p := \frac{L^2}{k} \tag{3.34}$$

expression (3.33) reduces to

$$r = \frac{p}{1 + \epsilon\cos\varphi} \tag{3.35}$$

Equation (3.35) is the focal equation of a conic. The parameter ϵ is called the eccentricity of the conic, which determines the type of conic according to the table in Figure 1. It is also possible to determine the type of orbit according to the values of E. To that end, the parameter $E_{\min}$ is introduced. $E_{\min}$ is defined as the value of energy for which the eccentricity ϵ is 0. According to (3.34), that is

$$E_{\min} := -\frac{k^2}{2L^2} \tag{3.36}$$

Remark 3.2. *We have seen that the relative position vector $\boldsymbol{r} := \boldsymbol{r}_2 - \boldsymbol{r}_1$ has its orbit in a conic. As in a barycentric reference frame both $\boldsymbol{r}_1, \boldsymbol{r}_2$ are multiples of $\boldsymbol{r}$* (3.2)*, their trajectories are scaled conics of the same type.*

To sum up, all the possible types of orbits in the Kepler problem have been described and classified in terms of the energy E, according to Figure 1. As it has been seen in Remark 3.2, this also gives the same possible types of orbits and classification in the Two-Body Problem. We also recall that equations (3.26) and (3.27) gave a solution for Kepler's problem, up to the computation of the corresponding integrals.

To complete the study of the Two-Body Problem, we include the classical Kepler laws. We will not give a proof of them, we refer the reader to [1] or [9].

Kepler's 1st law: The planets move in elliptic orbits with the sun in one of its foci.

Kepler's 2nd law: The radius that joints the planet with the Sun sweeps equal areas in equal times.

Kepler's 3rd law: The square of the period T of the planet is proportional to the cube of the semi-major axes a of the ellipse. More specifically,

$$T^2 = \frac{4\pi^2}{G(m_1 + m_2)} a^3 \tag{3.37}$$

Remark 3.3. *Kepler's laws refer only to the elliptic motion.*

4 The Planar and Circular Restricted Three-Body Problem

The Restricted Three-Body Problem is a simplified model for the Three-Body Problem. It consists on assuming that one of the bodies, namely the third body, has such a small mass that its effect on the motion of the two other bodies (the primaries) can be neglected. Thus, the primaries behave as in the Two-Body Problem, which has already been described in the previous section. What still remains unknown is the motion of the third body.

To study the motion of the third body, we will focus on a particular case, the so-called Planar and Circular Restricted Three-Body Problem (PCR3BP). It is further assumed that the motion of the third body takes place in the same plane where the primaries move (planar) and that the motion of the primaries takes place in circles around its common barycenter (circular).

Remark 4.1. *If the mass of the third body is neglected, the barycenter of the system is considered to be the barycenter of the primaries.*

To deal with the Planar and Circular Restricted Three-Body Problem we will follow a Hamiltonian mechanics approach. The main references in the first three sections of this chapter are [6] and [14].

4.1 Equations of motion

Let B_1, B_2, B_3 be the three bodies, being B_1 the most massive body and B_3 the less massive one. We will also refer to them as the first, the second and the third body. Let M_1, M_2, M_3 be their corresponding masses.

4.1.1 Cartesian sidereal barycentric coordinates

Consider a reference frame $\{O; \boldsymbol{x}, \boldsymbol{y}, \boldsymbol{z}\}$ centered at the barycenter, with the x-axis pointing to B_1 at time $\tau = 0$, the y-axis orthogonal to it in the plane of motion and oriented in such a way that the first body crosses first its positive part and the z-axis orthogonal to the plane of motion. Let $\boldsymbol{R}_1, \boldsymbol{R}_2, \boldsymbol{R}_3$ be the position vectors of the corresponding bodies in the reference frame. Assume that B_1, B_2 move in circles around its common barycenter and that the motion of B_3 takes place in the plane of motion of the primaries.

From (2.13), taking into account the restricted assumption, the vectorial equation of motion for the third body is

$$\ddot{\boldsymbol{R}}_3 = -G\frac{M_1}{R_{13}^3}\boldsymbol{R}_{13} - G\frac{M_2}{R_{23}^3}\boldsymbol{R}_{23} \tag{4.1}$$

In order to simplify and clarify further development, it is convenient to introduce units of time, distance and mass such that the gravitational constant G is 1, the

distance between the primaries is 1 and the total mass of the primaries, $M_1 + M_2$, is also 1. To that end, we introduce new variables in time t, position (x_i, y_i) and mass m_j, defined by

$$\alpha t = \tau; \qquad \beta(x_i, y_i) = (X_i, Y_i) \quad i = 1, 2, 3; \qquad \gamma m_j = M_j \quad j = 1, 2 \tag{4.2}$$

The change of variables in positions and mass leads to

$$\frac{d^2 x_3}{d\tau^2} = \frac{d^2}{d\tau^2}\left[\frac{1}{\beta} X_3\right] = \frac{G\gamma}{\beta^3}\left[-\frac{m_1}{r_{13}^3}(x_3 - x_1) - \frac{m_2}{r_{23}^3}(x_3 - x_2)\right]$$

where $r_{ij}^2 = (x_j - x_i)^2 + (y_j - y_i)^2$. Introducing the time scaling $\tau = \alpha t$, we get

$$\frac{d^2}{dt^2}\Big[x_3\Big] = \alpha^2 \frac{d^2}{d\tau^2}[x_3(\tau(t))] = \frac{\alpha^2 G\gamma}{\beta^3}\left[-\frac{m_1}{r_{13}^3}(x_3 - x_1) - \frac{m_2}{r_{23}^3}(x_3 - x_2)\right] \tag{4.3}$$

The change of variables for y_3 is done identically. We choose the parameters α, β and γ in the following way

$$1 = m_1 + m_2 = \frac{1}{\gamma}(M_1 + M_2) \Rightarrow \gamma = M_1 + M_2$$

$$1 = r_{12} = \sqrt{(x_2 - x_1)^2 + (y_2 - y_1)^2} = \frac{1}{\beta} R_{12} \Rightarrow \beta = R_{12}$$

$$1 = \frac{\alpha^2 G\gamma}{\beta^3} \Rightarrow \alpha = \sqrt{\frac{\beta^3}{G\gamma}}$$

We define $m := m_2 \in [0, 0.5]$, so $m_1 = 1 - m$. The vectorial equation of motion for the third body after this change of variables is

$$\ddot{\boldsymbol{r}}_3 = -\frac{1-m}{r_{13}^3}\boldsymbol{r}_{13} - \frac{m}{r_{23}^3}\boldsymbol{r}_{23} \tag{4.4}$$

We are now interested in describing the position of the primaries after the change of variables. From (3.3), as the center of mass $\boldsymbol{R}$ is at the origin

$$\boldsymbol{r}_1 = -m\boldsymbol{r}_{12}; \qquad \boldsymbol{r}_2 = (1-m)\boldsymbol{r}_{12} \tag{4.5}$$

So $\boldsymbol{r}_1, \boldsymbol{r}_2$ are linearly dependent, with opposite directions and thus $1 = r_{12} = r_1 + r_2$. Furthermore, from the circular assumption, r_1, r_2 are constant. More specifically,

$$r_1 = m; \qquad r_2 = 1 - m \tag{4.6}$$

according to (4.5). According to (3.17), this is, $L = r_{12}^2 \dot{\varphi}$, the primaries move at constant angular velocity $\omega := \dot{\varphi}$. From Kepler's third law, (3.37), we deduce that this constant is 1, as $m_1 + m_2 = 1$, $G = 1$, and the semi-major axis a of the ellipse described by the second body with the first body in one of its foci, which in this case is a circle, is $a = r_{12} = 1$. So (3.37) reduces to

$$\omega = \frac{2\pi}{T} = 1$$

See Figure 2 for a geometric description of the motion of the primaries. Analytically, its positions at time t are

$$\begin{aligned} \boldsymbol{r}_1(t) &= (x_1(t), y_1(t)) = m(\cos t, \sin t) \\ \boldsymbol{r}_2(t) &= (x_2(t), y_2(t)) = -(1-m)(\cos t, \sin t) \end{aligned} \tag{4.7}$$

We derive now the Hamiltonian and the corresponding Hamilton equations for the third body in these coordinates.

To simplify notation, we denote $(x(t), y(t)) := (x_3(t), y_3(t)) = \boldsymbol{r}_3$ and $(\dot{x}(t), \dot{y}(t)) := (\dot{x}_3(t), \dot{y}_3(t)) = \dot{\boldsymbol{r}}_3$.

By definition, the Lagrangian L is

$$L = T - U = \frac{1}{2} m_3(\dot{x}^2 + \dot{y}^2) + \frac{G m_1 m_3}{r_{13}} + \frac{G m_2 m_3}{r_{23}} = \frac{1}{2} m_3(\dot{x}^2 + \dot{y}^2) + \frac{(1-m) m_3}{r_{13}} + \frac{m m_3}{r_{23}}$$

where

$$\begin{aligned} r_{13} &:= |\boldsymbol{r}_3 - \boldsymbol{r}_1| = [(x(t) - m\cos t)^2 + (y(t) - m \sin t)^2]^{1/2} \\ r_{23} &:= |\boldsymbol{r}_3 - \boldsymbol{r}_2| = [(x(t) + (1-m)\cos t)^2 + (y(t) + (1-m)\sin t)^2]^{1/2} \end{aligned} \tag{4.8}$$

As the Lagrange and Hamilton equations are independent of multiplicative constants appearing in the Lagrangian and Hamiltonian, we should cancel m_3 and get

$$L = \frac{1}{2}(\dot{x}^2 + \dot{y}^2) + \frac{(1-m)}{r_{13}} + \frac{m}{r_{23}} \tag{4.9}$$

Introducing the associated momenta

$$\boldsymbol{p} = (p_x, p_y) := \left(\frac{\partial L}{\partial \dot{x}}, \frac{\partial L}{\partial \dot{y}} \right) = (\dot{x}, \dot{y}) \tag{4.10}$$

the corresponding Hamiltonian is

$$H = H(x, y, p_x, p_y, t) := p_x \dot{x} + p_y \dot{y} - L = \frac{1}{2}(p_x^2 + p_y^2) - \frac{(1-m)}{r_{13}} - \frac{m}{r_{23}} \tag{4.11}$$

and the Hamilton equations are

$$\begin{aligned} \dot{x} &= \frac{\partial H}{\partial p_x} = p_x; \qquad & \dot{p}_x &= -\frac{\partial H}{\partial x} = -(1-m)\frac{x - m\cos t}{r_{13}^3} - m\frac{x + (1-m)\cos t}{r_{23}^3} \\ \dot{y} &= \frac{\partial H}{\partial p_y} = p_y; \qquad & \dot{p}_y &= -\frac{\partial H}{\partial y} = -(1-m)\frac{y - m\sin t}{r_{13}^3} - m\frac{y + (1-m)\sin t}{r_{23}^3} \end{aligned} \tag{4.12}$$

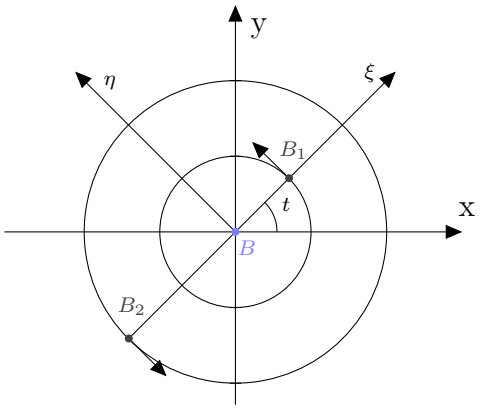

Figure 2: Sidereal and synodical barycentric coordinates. Motion of the primaries B_1, B_2.

4.1.2 Cartesian synodical barycentric coordinates

In the Cartesian sidereal barycentric reference frame, the primaries move at constant angular velocity 1 around the barycenter. In order to fix the primaries, consider a reference frame $\{O; \boldsymbol{\xi}, \boldsymbol{\eta}, \boldsymbol{\kappa}\}$, with the origin at the barycenter, such that the ξ, η axes move at constant angular velocity 1 with respect to the Cartesian sidereal reference frame $\{O; \boldsymbol{x}, \boldsymbol{y}, \boldsymbol{z}\}$. Let $(\xi_i, \eta_i, \kappa_i = 0)$, or (ξ_i, η_i) for short, and (p_{ξ_i}, p_{η_i}) be the coordinates and the associated momenta of the i-th body in $\{O; \boldsymbol{\xi}, \boldsymbol{\eta}, \boldsymbol{\kappa}\}$. Assume also that at time $t = 0$ both reference frames coincide. See Figure 2 for an interpretation of it.

The transformation of coordinates from $\{O; \boldsymbol{\xi}, \boldsymbol{\eta}, \boldsymbol{\kappa}\}$ to $\{O; \boldsymbol{x}, \boldsymbol{y}, \boldsymbol{z}\}$ is given, at time t, by a rotation $\mathcal{R}_{-t}$ of angle $-t$, namely

$$\begin{pmatrix} \xi \\ \eta \end{pmatrix} = \mathcal{R}_{-t} \begin{pmatrix} x \\ y \end{pmatrix} = \begin{pmatrix} \cos t & \sin t \\ -\sin t & \cos t \end{pmatrix} \begin{pmatrix} x \\ y \end{pmatrix} = \begin{pmatrix} x \cos t & + & y \sin t \\ -x \sin t & + & y \cos t \end{pmatrix} \tag{4.13}$$

Following from (4.7), the position of the primaries is

$$\begin{pmatrix} \xi_1 \\ \eta_1 \end{pmatrix} = \begin{pmatrix} m \\ 0 \end{pmatrix}; \qquad \begin{pmatrix} \xi_2 \\ \eta_2 \end{pmatrix} = \begin{pmatrix} -(1-m) \\ 0 \end{pmatrix} \tag{4.14}$$

To obtain the equations of motion, we will use canonical transformations introduced by means of time-dependent generating functions, so that a new Hamiltonian which preserves the Hamilton equation structure is obtained. We will consider a generating function of the form

$$F = F(x, y, p_\xi, p_\eta, t) \tag{4.15}$$

If it holds

$$p_x = \frac{\partial F}{\partial x}; \qquad p_y = \frac{\partial F}{\partial y} \tag{4.16}$$

and

$$\xi = \frac{\partial F}{\partial p_\xi}; \qquad \eta = \frac{\partial F}{\partial p_\eta} \tag{4.17}$$

the equations in the new reference frame are Hamiltonian, with Hamiltonian H^* given by

$$H^*(\xi, \eta, p_\xi, p_\eta, t) = H(x, y, p_x, p_y, t) + \frac{\partial F}{\partial t} \tag{4.18}$$

Consider the generating function

$$F(x, y, p_\xi, p_\eta, t) = \xi(x, y, t)p_\xi + \eta(x, y, t)p_\eta = (x\cos t + y\sin t)p_\xi + (-x\sin t + y\cos t)p_\eta \tag{4.19}$$

which satisfies the conditions in (4.17). If we impose (4.16), we get

$$\begin{pmatrix} p_x \\ p_y \end{pmatrix} = \mathcal{R}_t \begin{pmatrix} p_\xi \\ p_\eta \end{pmatrix}; \qquad \begin{pmatrix} p_\xi \\ p_\eta \end{pmatrix} = \mathcal{R}_{-t} \begin{pmatrix} p_x \\ p_y \end{pmatrix} = \begin{pmatrix} p_x\cos t & + & p_y\sin t \\ -p_x\sin t & + & p_y\cos t \end{pmatrix} \tag{4.20}$$

So, according to (4.18), the Hamiltonian H_1 in Cartesian barycentric coordinates, which results to be time-independent, is

$$H_1(\xi, \eta, p_\xi, p_\eta) = \frac{1}{2}(p_\xi^2 + p_\eta^2) + \eta p_\xi - \xi p_\eta - \frac{1-m}{\rho_1} - \frac{m}{\rho_2} \tag{4.21}$$

where ρ_1, ρ_2 denote the distance between the primaries and the third body, namely

$$\rho_1^2 = (\xi - m)^2 + \eta^2; \qquad \rho_2^2 = (\xi + 1 - m)^2 + \eta^2 \tag{4.22}$$

The Hamilton equations are then

$$\begin{aligned} \dot{\xi} &= \frac{\partial H_1}{\partial p_\xi} = p_\xi + \eta; \quad \dot{p}_\xi = -\frac{\partial H_1}{\partial \xi} = p_\eta - (1-m)\frac{\xi - m}{\rho_1^3} - m\frac{\xi + 1 - m}{\rho_2^3} \\ \dot{\eta} &= \frac{\partial H_1}{\partial p_\eta} = p_\eta - \xi; \quad \dot{p}_\eta = -\frac{\partial H_1}{\partial \eta} = -p_\xi - (1-m)\frac{\eta}{\rho_1^3} - m\frac{\eta}{\rho_2^3} \end{aligned} \tag{4.23}$$

or, equivalently, in terms of two second order differential equations

$$\begin{aligned} \ddot{\xi} &= 2\dot{\eta} + \xi - (1-m)\frac{\xi - m}{\rho_1^3} - m\frac{\xi + 1 - m}{\rho_2^3} \\ \ddot{\eta} &= -2\dot{\xi} + \eta - (1-m)\frac{\eta}{\rho_1^3} - m\frac{\eta}{\rho_2^3} \end{aligned} \tag{4.24}$$

It is convenient to introduce the function

$$\Omega(\xi, \eta) = \frac{1}{2}(\xi^2 + \eta^2) + \frac{1-m}{\rho_1} + \frac{m}{\rho_2} \tag{4.25}$$

so that equations (4.24) can be written as

$$\ddot{\xi} - 2\dot{\eta} = \frac{\partial \Omega}{\partial \xi}; \qquad \ddot{\eta} + 2\dot{\xi} = \frac{\partial \Omega}{\partial \eta} \tag{4.26}$$

4.1.3 Polar synodical barycentric coordinates

For future development, it is convenient to introduce polar synodical coordinates in the plane of motion. They are defined as

$$\rho = \rho(\xi, \eta) := \sqrt{\xi^2 + \eta^2}; \qquad \theta = \theta(\xi, \eta) := \operatorname{atan}\left(\frac{\eta}{\xi}\right) \tag{4.27}$$

We denote by p_ρ, p_θ the associated momenta. We will obtain the new equations of motion by means of a time-independent generating function. In this case, consider the generating function F defined by

$$F = F(\xi, \eta, p_\rho, p_\theta) = \rho(\xi, \eta)p_\rho + \theta(\xi, \eta)p_\theta = \sqrt{\xi^2 + \eta^2}p_\rho + \operatorname{atan}\left(\frac{\eta}{\xi}\right)p_\theta \tag{4.28}$$

The analogous condition of (4.17) is rapidly checked, while the analogous condition of (4.16) leads to

$$p_\xi = \frac{\partial F}{\partial \xi} = \frac{\xi}{\rho}p_\rho - \frac{\eta}{\rho^2}p_\theta; \qquad p_\eta = \frac{\partial F}{\partial \eta} = \frac{\eta}{\rho}p_\rho + \frac{\xi}{\rho^2}p_\theta \tag{4.29}$$

As F is time independent, following from (4.18), the Hamiltonian H_2 in polar barycentric coordinates is given by

$$H_2(\rho, \theta, p_\rho, p_\theta) = H_1(\xi, \eta, p_\xi, p_\eta) = \frac{1}{2}\left(p_\rho^2 + \frac{p_\theta^2}{\rho^2}\right) - p_\theta - (1-m)\frac{1}{\rho_1} - m\frac{1}{\rho_2} \tag{4.30}$$

where we have used the relations in (4.29) and ρ_1, ρ_2 are now given by

$$\rho_1^2 = \rho^2 - 2m\rho\cos\theta + m^2; \qquad \rho_2^2 = \rho^2 - 2(m-1)\rho\cos\theta + (m-1)^2 \tag{4.31}$$

The Hamilton equations are then

$$\begin{aligned} &\dot{\rho} = p_\rho; && \dot{p}_\rho = \frac{p_\theta^2}{\rho^3} - (1-m)\frac{\rho - m\cos\theta}{\rho_1^3} - m\frac{\rho + (1-m)\cos\theta}{\rho_2^3} \\ &\dot{\theta} = \frac{p_\theta}{\rho^2} - 1; && \dot{p}_\theta = -m(1-m)\rho\sin\theta\left(\frac{1}{\rho_1^3} - \frac{1}{\rho_2^3}\right) \end{aligned} \tag{4.32}$$

4.2 Equilibrium solutions

An important feature of the equations in the Cartesian barycentric synodical framework is that they admit equilibrium solutions. As the synodical reference framework is rotating at constant angular velocity 1 with respect to the sidereal one, the equilibrium solutions correspond to periodic orbits in the sidereal framework. They are called Lagrangian equilibrium solutions or, equivalently, Lagrangian equilibrium points, and denoted by L_1, L_2, L_3, L_4 and L_5.

4.2.1 Lagrangian equilibrium solutions

To obtain them, consider the equations in Cartesian synodical barycentric coordinates (4.24) and impose the conditions $\ddot{\xi} = \dot{\xi} = \ddot{\eta} = \dot{\eta} = 0$ for equilibrium solutions

$$\begin{aligned} \xi - (1-m)\frac{\xi - m}{\rho_1^3} - m\frac{\xi - m + 1}{\rho_2^3} = 0 \\ \eta - (1-m)\frac{\eta}{\rho_1^3} - m\frac{\eta}{\rho_2^3} = 0 \end{aligned} \tag{4.33}$$

Observe that the second of (4.33) has η as a common factor, and thus we shall distinguish two cases.

Case 1: $\eta = 0$

The first one of (4.33) becomes

$$\xi - (1-m)\frac{\xi - m}{|\xi - m|^3} - m\frac{\xi - m + 1}{|\xi - m + 1|^3} = \xi - (1-m)\frac{\sigma(\xi - m)}{|\xi - m|^2} - m\frac{\sigma(\xi - m + 1)}{|\xi - m + 1|^2} = 0$$

where σ denotes the sign function. The above expression is equivalent to

$$\xi(\xi-m)^2(\xi-m+1)^2-(1-m)(\xi-m+1)^2\sigma(\xi-m)-m(\xi-m)^2\sigma(\xi-m+1) = 0 \tag{4.34}$$

which represents three different quintic equations, depending on whether $\xi < m-1$ or $m-1 \leq \xi < m$ or $\xi \leq m$. In every case, from (4.34) we obtain

(i) $m - 1 \leq \xi < m$

$$p_1(\xi) := \xi(\xi - m)^2(\xi - m + 1)^2 + (1 - m)(\xi - m + 1)^2 - m(\xi - m)^2 = 0 \tag{4.35}$$

As $p_1(m-1) = -m \leq 0$ and $p_1(0) = (1-m)^3 - m^3 \geq 0$, according to Bolzano's theorem, there exists $\alpha_1 \in [m-1, 0] \subseteq [m-1, m]$ such that $p_1(\alpha_1) = 0$. So, at least exists one equilibrium solution with ξ-coordinate in $[m-1, m]$. We call it $L_1 := (\alpha_1, 0)$.

In the remaining cases, Bolzano's theorem also gives the existence of at least an equilibrium solution, as

(ii) $\xi \leq m - 1$

$$p_2(\xi) := \xi(\xi - m)^2(\xi - m + 1)^2 + (1 - m)(\xi - m + 1)^2 + m(\xi - m)^2 = 0 \tag{4.36}$$

which satisfies $p_2(m-1) = m > 0$ and $p_2(\xi) \longrightarrow -\infty$ as $\xi \longrightarrow -\infty$. We call the corresponding equilibrium solution $L_2 := (\alpha_2, 0)$.

(iii) $\xi \geq m$

$$p_3(\xi) := \xi(\xi - m)^2(\xi - m + 1)^2 - (1 - m)(\xi - m + 1)^2 - m(\xi - m)^2 = 0 \tag{4.37}$$

which satisfies $p_3(m) = m - 1 < 0$ and $p_3(\xi) \longrightarrow +\infty$ as $\xi \longrightarrow +\infty$. We call the corresponding equilibrium solution $L_3 := (\alpha_3, 0)$.

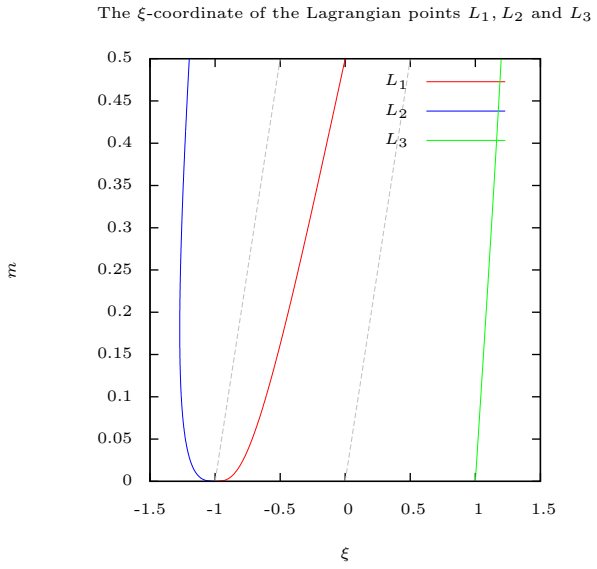

Figure 3: L_1, L_2, L_3 for different values of m. In grey, ξ-coordinates of the primaries.

As the previous equations are quintic equations, we should not expect to solve them explicitly in terms of radicals. However, the solutions can be approximated numerically for any value of m. We should do the computations for some values of m, to get an idea of the behaviour.

For the numerical computations, see Figure 3. We used Newton's method to find the roots of the polynomials p_i, making sure that the roots are in the interval of interest in every case. If we fix a value of m, we get the ξ-coordinate of the three Lagrangian points L_1, L_2 and L_3 by intersecting the curves in the figure with the horizontal line $y = m$.

We observe that, as the mass m of the second body increases, the L_1 point is placed further away from the second body, reaching the middle point between the primaries when the mass value is $m = 0.5$. This is logical, as an increase on the mass m suppose a lower effect of the first body and a greater of the second, so to obtain again an equilibrium the third body should get a bit closer to the first body. In the case $m = 0.5$, as both primaries do the same gravitational force on the third, the equilibrium is reached in the middle point between them.

We also observe that, as the mass m increases, L_2 gets further away from the second body, while L_3 gets closer to the first body. Similar interpretations justify these results.

Case 2: $\eta \neq 0$

The second equation of (4.33) reduces to

$$1 - \frac{1-m}{\rho_1^3} - \frac{m}{\rho_2^3} = 0 \tag{4.38}$$

Multiplying (4.38) by $(\xi - m)$ and subtracting the equations in (4.33), we obtain

$$m - \frac{m}{\rho_2^3} = 0 \Leftrightarrow m = 0 \text{ or } \rho_2 = 1$$

Multiplying this time by $(\xi - m + 1)$, we obtain

$$(1-m)\left(1 - \frac{1}{\rho_1^3}\right) = 0 \Leftrightarrow \rho_1 = 1$$

Recalling the definition of ρ_1, ρ_2 given in (4.22), and using the conditions from above, in the case $m \neq 0$ we get

$$\rho_2^2 = \rho_1^2 = 1 \Leftrightarrow (\xi - m + 1)^2 = (\xi - m)^2 \Leftrightarrow 2(\xi - m) + 1 = 0$$

Thus, $\xi = m - \frac{1}{2}$ and $\eta = \pm\frac{\sqrt{3}}{2}$. The Lagrangian points L_4 and L_5 are then defined

$$L_4 := \left(m - \frac{1}{2}, \frac{\sqrt{3}}{2}\right); \qquad L_5 := \left(m - \frac{1}{2}, -\frac{\sqrt{3}}{2}\right) \tag{4.39}$$

For $m = 0$ the first condition is always satisfied, so the remaining condition $\rho_1 = 1$ leads to a set of equilibrium solutions on a circle. Observe that this corresponds to the circular solution for Kepler's problem ($\epsilon = 0$). The fact that all the solutions on the circle ρ_1 are equally valid corresponds to different initial positions on the circle. This makes sense, because if $m = 0$, the Restricted Three-Body Problem reduces to Kepler's problem.

Remark 4.2. *Find an example of the location of the Lagrangian points for $m = 0.3$ in Figure 6. They are represented by black dots. L_4 and L_5 correspond to the points with non-zero η-coordinate, whereas L_1, L_2 and L_3 are collinear to the primaries and appear in the following order, from left to right: L_2, L_1, L_3.*

Regarding the uniqueness, from the deduction of the existence of the Lagrangian equilibrium solutions we get that L_4 and L_5 are the only non-collinear equilibrium solutions (Case 2). It remains unknown whether other collinear solutions can exist. The following proposition gives the non-existence of other collinear solutions.

Proposition 4.1. *L_1, L_2 and L_3 are the only collinear equilibrium solutions. Thus, all the equilibrium solutions of the system in Cartesian synodical barycentric coordinates are the Lagrangian equilibrium solutions.*

Proof. Following from (4.33), as $\eta = 0$, we get

$$\xi = (1-m)\frac{\sigma(\xi - m)}{(\xi - m)^2} + m\frac{\sigma(\xi - m + 1)}{(\xi - m + 1)^2} \tag{4.40}$$

As we have done previously, we shall consider the three following cases

(i) $m - 1 \leq \xi \leq m$

The right hand side of (4.40) is strictly decreasing in $(m-1, m)$, as its derivative is

$$2(1-m)(\xi-m)^{-3} - 2m(\xi-m+1)^{-3} < 0 \quad \forall \xi \in (m-1, m)$$

As the left hand side is strictly increasing, there is only one possible intersecting point, namely L_1, as we have already proved its existence.

The other cases are analogous, as the derivatives of the right hand side of (4.40) in $(-\infty, m-1)$ and $(m, +\infty)$ are, respectively

$$2(1-m)(\xi-m)^{-3} + 2m(\xi-m+1)^{-3} < 0 \quad \forall \xi \in (-\infty, m-1)$$

and

$$-2(1-m)(\xi-m)^{-3} - 2m(\xi-m+1)^{-3} < 0 \quad \forall \xi \in (m, +\infty)$$

□

4.2.2 Stability of the Lagrangian equilibrium solutions

We study now the stability of the Lagrangian equilibria. Following from (4.26), and introducing the velocities $v_\xi := \dot{\xi}, v_\eta := \dot{\eta}$, we get the vector field F, defined by

$$\begin{array}{rcl} \dot{\xi} & = & v_\xi \\ \dot{\eta} & = & v_\eta \\ \dot{v}_\xi & = & 2v_\eta + \Omega_\xi \\ \dot{v}_\eta & = & -2v_\xi + \Omega_\eta \end{array} \tag{4.41}$$

where $\Omega_\xi := \frac{\partial \Omega}{\partial \xi}$ and $\Omega_\eta := \frac{\partial \Omega}{\partial \eta}$. The Jacobian matrix of F is

$$DF := \begin{pmatrix} 0 & 0 & 1 & 0 \\ 0 & 0 & 0 & 1 \\ \Omega_{\xi\xi} & \Omega_{\xi\eta} & 0 & 2 \\ \Omega_{\eta\xi} & \Omega_{\eta\eta} & -2 & 0 \end{pmatrix} \tag{4.42}$$

Computing from the definition of Ω in (4.25)

$$\begin{aligned} \Omega_\xi &= \xi - (1-m)\frac{\xi-m}{\rho_1^3} - m\frac{\xi+1-m}{\rho_2^3}; \qquad \Omega_\eta = \eta - (1-m)\frac{\eta}{\rho_1^3} - m\frac{\eta}{\rho_2^3} \\ \Omega_{\xi\xi} &= 1 - (1-m)\frac{\eta^2 - 2(\xi-m)^2}{\rho_1^5} - m\frac{\eta^2 - 2(\xi+1-m)^2}{\rho_2^5} \\ \Omega_{\xi\eta} &= \frac{3(1-m)(\xi-m)\eta}{\rho_1^5} + \frac{3m(\xi+1-m)\eta}{\rho_2^5} \\ \Omega_{\eta\eta} &= 1 - (1-m)\frac{(\xi-m)^2 - 2\eta^2}{\rho_1^5} - m\frac{(\xi+1-m)^2 - 2\eta^2}{\rho_2^5} \end{aligned} \tag{4.43}$$

The characteristic polynomial is

$$\det(DF - \lambda I) = \lambda^4 + (-\Omega_{\xi\xi} - \Omega_{\eta\eta} + 4)\lambda^2 + (\Omega_{\xi\xi}\Omega_{\eta\eta} - \Omega_{\xi\eta}^2) \tag{4.44}$$

As the characteristic equation $\det(DF - \lambda I) = 0$ is biquadratic, its roots are

$$\lambda_{\pm} = \pm\frac{1}{\sqrt{2}}\Big[\Omega_{\xi\xi} + \Omega_{\eta\eta} - 4 - [(\Omega_{\xi\xi} + \Omega_{\eta\eta} - 4)^2 - 4(\Omega_{\xi\xi}\Omega_{\eta\eta} - \Omega_{\xi\eta}^2)]^{1/2}\Big]^{1/2}$$

$$\mu_{\pm} = \pm\frac{1}{\sqrt{2}}\Big[\Omega_{\xi\xi} + \Omega_{\eta\eta} - 4 + [(\Omega_{\xi\xi} + \Omega_{\eta\eta} - 4)^2 - 4(\Omega_{\xi\xi}\Omega_{\eta\eta} - \Omega_{\xi\eta}^2)]^{1/2}\Big]^{1/2} \quad (4.45)$$

To study the stability of the equilibrium points, the fact that $\lambda \in \text{spec}(DF) \Leftrightarrow -\lambda \in \text{spec}(DF)$ plays a crucial role. If there exists an eigenvalue $\lambda \in \text{spec}(DF)$ such that $\text{Re}\lambda \neq 0$, there exists an eigenvalue with positive real part (either λ or $-\lambda$). Thus, a necessary condition for the equilibrium points to be spectrally stable is that all four eigenvalues are purely imaginary.

Remark 4.3. *We recall the following stability criteria for ODE's regarding the purely imaginary eigenvalues:*

Let A be the Jacobian matrix associated to a system of ODE's, evaluated at an equilibrium solution p. Assume that $\forall\lambda \in specA\ Re\lambda \leq 0$, that is, p is spectrally stable. Then,

p is linearly stable $\Leftrightarrow \forall\lambda \in specA \cap \{Re\lambda = 0\}$, λ has multiplicity one as an eigenvalue of A.

Case 1: Stability of L_1, L_2, L_3

As L_1, L_2, L_3 lie on the ξ-axes, they satisfy the condition $\eta = 0$. We shall introduce the quantity

$$\zeta := \frac{1-m}{\rho_1^3} + \frac{m}{\rho_2^3} \quad (4.46)$$

to make the discussion easier. Taking into account $\eta = 0$ and evaluating (4.43) in (4.44) we obtain the characteristic polynomial (4.44) in terms of ζ

$$\lambda^4 + (2-\zeta)\lambda^2 + (1 + \zeta - 2\zeta^2) \quad (4.47)$$

Due to the biquadratic form of equation (4.47), we recall that the only possibility to have spectral stability is that all eigenvalues are purely imaginary. Assume that there is spectral stability. As $\lambda_- = -\lambda_+$, $\mu_- = -\mu_+$ and are purely imaginary, the determinant of DF is

$$\det DF = (1 + \zeta - 2\zeta^2) = \lambda_+\lambda_-\mu_+\mu- = (-\lambda_+^2)(-\mu_+^2) \geq 0$$

The polynomial $-2\zeta^2 + \zeta + 1$ has roots $-1/2$ and 1, so the values of ζ that satisfy $-2\zeta^2 + \zeta + 1 \geq 0$ are $-1/2 \leq \zeta \leq 1$.

On the other hand, rearranging the first equilibrium condition (4.33), we get

$$\xi\left(1 - \frac{1-m}{\rho_1^3} - \frac{m}{\rho_2^3}\right) + \frac{m(1-m)}{\rho_1^3} - \frac{m(1-m)}{\rho_2^3} = \xi(1-\zeta) + m(1-m)\left(\frac{1}{\rho_1^3} - \frac{1}{\rho_2^3}\right) = 0$$

So,

$$(1-\zeta) = \frac{m(1-m)}{\xi}\left(\frac{1}{\rho_2^3} - \frac{1}{\rho_1^3}\right) \quad (4.48)$$

Now we will show that for L_1, L_2, L_3 the value of ζ is greater than 1, and so there is a contradiction with the condition $-\frac{1}{2} \leq \zeta \leq 1$.

For L_1, as $\rho_1 < 1, \rho_2 < 1$, directly from the definition of ζ (4.46)

$$\zeta = \frac{1-m}{\rho_1^3} + \frac{m}{\rho_2^3} > 1 - m + m = 1$$

For L_2, the ξ-coordinate is negative and $\rho_2 < \rho_1 \Rightarrow \frac{1}{\rho_1^3} < \frac{1}{\rho_2^3}$. From (4.48), we get $1 - \zeta < 0$ and thus $\zeta > 1$.

For L_3, following a similar argument as in the L_2 case, the ξ-coordinate is positive and $\frac{1}{\rho_2^3} - \frac{1}{\rho_1^3}$ is negative, so $\zeta > 1$.

Therefore, we can conclude that L_1, L_2, L_3 are unstable for all values of m.

Case 2: Stability of L_4, L_5

Evaluating the coordinates of L_4 (4.39) on (4.43) and (4.45), we get

$$\Omega_{\xi\xi} = \frac{3}{4}; \qquad \Omega_{\xi\eta} = \frac{3\sqrt{3}}{4}(2m-1); \qquad \Omega_{\eta\eta} = \frac{9}{4}$$

$$\lambda_{\pm} = \pm\frac{1}{\sqrt{2}}\sqrt{-1 - \sqrt{1 - 27m(1-m)}}; \qquad \mu_{\pm} = \pm\frac{1}{\sqrt{2}}\sqrt{-1 + \sqrt{1 - 27m(1-m)}} \tag{4.49}$$

Regarding L_5, the only difference is on $\Omega_{\xi\eta}$, which changes its sign. As it does not have any effect on the eigenvalues, from now on everything is valid for both equilibrium points.

So, $\lambda_{\pm}, \mu_{\pm}$ are purely imaginary if, and only if $0 \leq 1 - 27m(1-m) \leq 1$. This is equivalent to $0 \leq 27m(1-m) \leq 1$.

For $m \in [0, 0.5]$, the inequality $0 \leq 27m(1-m)$ is always satisfied. Regarding the second inequality, the equation $27m(1-m) - 1 = -27m^2 + 27m - 1 = 0$ admits two solutions

$$m_+ = \frac{1 - \sqrt{23/27}}{2}; \qquad m_- = \frac{1 + \sqrt{23/27}}{2} \tag{4.50}$$

Thus, the inequality is satisfied in $(-\infty, m_+)$ and $(m_-, +\infty)$, but as $m \in [0, 0.5]$, we conclude that L_4, L_5 are spectrally stable if, and only if

$$0 \leq m \leq \frac{1 - \sqrt{23/27}}{2} \simeq 0.0385 \tag{4.51}$$

According to Remark 4.3, as the eigenvalues are all different if, and only if $1 - 27m(1-m) \notin \{0, 1\}$ (see (4.49)), L_4, L_5 are linearly stable if, and only if the strict inequalities in (4.51) are satisfied.

4.3 The Jacobi integral. Hill's regions

The first integrals of the general n-Body Problem need not to be first integrals of the Planar and Circular Restricted 3-Body Problem. This is a direct consequence

of the "restricted" assumption, as the third body does not make an effect on the two primaries, while the primaries do definitely have an effect on the third body. However, it does exists a first integral, namely the Jacobi integral. Furthermore, the Jacobi integral gives topological conditions on the places where the motion of the third body can take place, the so-called Hill regions.

The Hamiltonian H_1 in the barycentric synodical reference frame (4.21)

$$H_1(\xi, \eta, p_\xi, p_\eta, t) = \frac{1}{2}(p_\xi^2 + p_\eta^2) + \eta p_\xi - \xi p_\eta - \frac{1-m}{\rho_1} - \frac{m}{\rho_2}$$

does not depend explicitly on time. So, according to

$$\frac{dH_1}{dt} = \frac{\partial H_1}{\partial t} \tag{4.52}$$

the Hamiltonian is a first integral.

Def 4.1. *The Jacobi integral or Jacobi constant is*

$$C := -2H_1 \tag{4.53}$$

It is clear that it is a first integral equivalent to H_1.

Proposition 4.2.

$$2\Omega(\xi, \eta) - C = \dot{\xi}^2 + \dot{\eta}^2 =: v^2 \tag{4.54}$$

where Ω is the function introduced in (4.25) and v is the modulus of the velocity.

Proof. Direct computations, using the Hamilton equations (4.23), show

$$2\Omega - C = \xi^2 + \eta^2 + p_\xi^2 + p_\eta^2 + 2\eta p_\xi - 2\xi p_\eta = \dot{\xi}^2 + \dot{\eta}^2$$

□

The quantity v^2 is always greater or equal 0, so as the function $\Omega = \Omega(\xi, \eta)$ is only a function of the positions, the motion of the third body can only take place in the regions where

$$2\Omega(\xi, \eta) - C \geq 0$$

Def 4.2. *Given a value of the Jacobi integral C, the Hill region is the set of values $(\xi, \eta) \in \mathbb{R}^2$ for which the condition*

$$2\Omega(\xi, \eta) \geq C \tag{4.55}$$

holds.

Observe that an increase in the Jacobi integral implies that the corresponding Hill region becomes smaller, as the condition (4.55) is more restrictive.

4.3.1 Zero-velocity curves

Our next objective is to describe Hill's region. To that end, we will find its boundary, the zero-velocity curves.

Def 4.3. *Given a value of the Jacobi integral C, the zero velocity curves are the points $(\xi, \eta) \in \mathbb{R}^2$ that satisfy*

$$2\Omega(\xi, \eta) = C \tag{4.56}$$

Our objective is to determine the level curves of a function, namely

$$G(\xi, \eta) := 2\Omega(\xi, \eta) = \xi^2 + \eta^2 + 2\frac{1-m}{\rho_1} + 2\frac{m}{\rho_2} \tag{4.57}$$

A general method to find the level curves of a function $F : \mathbb{R}^2 \longrightarrow \mathbb{R}$ is provided, if F is smooth enough.

Davidenko method

Given a $\mathcal{C}^1$ function $F : \mathbb{R}^2 \longrightarrow \mathbb{R}$ and $k \in \mathbb{R}$, we want to describe the level curves of F at level k, namely

$$\{(x, y) \in \mathbb{R}^2 : F(x, y) = k\} \tag{4.58}$$

Introduce the arc parameter s to parametrize the curve $\gamma(s) = (x(s), y(s))$ whose trajectory is (4.58) (or a connected component of it). Thus, we have

$$F(x(s), y(s)) = k$$

Deriving the previous expression with respect to s

$$\frac{d}{ds}\big[F(x(s), y(s))\big] = F_x(x(s), y(s))\frac{dx}{ds} + F_y(x(s), y(s))\frac{dy}{ds} = 0 \tag{4.59}$$

where $F_x := \frac{\partial F}{\partial x}, F_y := \frac{\partial F}{\partial y}$. As the curve is parametrized by the arc parameter

$$1 = ||\gamma'(s)||^2 = \left(\frac{dx}{ds}\right)^2 + \left(\frac{dy}{ds}\right)^2 \tag{4.60}$$

Combining (4.59) and (4.60), we get

$$\left(\frac{dx}{ds}\right)^2 = \frac{F_y^2}{F_x^2 + F_y^2}; \qquad \left(\frac{dy}{ds}\right)^2 = \frac{F_x^2}{F_x^2 + F_y^2} \tag{4.61}$$

But, as $\frac{dx}{ds}, \frac{dy}{ds}$ satisfy (4.59), they must be of opposite sign, this is

$$\frac{dx}{ds} = \pm\frac{F_y}{\sqrt{F_x^2 + F_y^2}}; \qquad \frac{dy}{ds} = \mp\frac{F_x}{\sqrt{F_x^2 + F_y^2}} \tag{4.62}$$

So, according to (4.62), we have reduced the computation of the level curves of a function to the numerical integration of a system of differential equations.

	C_i
L_1	3.9201495841
L_2	3.5564130018
L_3	3.2913502189
L_4	2.7900000000
L_5	2.7900000000

Figure 4: Jacobi integral values C_i for which the Lagrangian points L_i are on the 0-velocity curve for $m = 0.3$.

Remark 4.4. *The function $G = 2\Omega$ (4.57) for which we want to find the level curves is not $\mathcal{C}^1$ in the positions of the primaries. However, this is not an inconvenient, as for a fixed real value of the Jacobi integral C, the values ρ_1, ρ_2 cannot be 0, because then the Jacobi integral would be ∞ (see (4.21)).*

In the case of interest to us, (4.62) needs the inputs

$$G_\xi = 2\xi - 2(1-m)\frac{\xi - m}{\rho_1^3} - 2m\frac{\xi + 1 - m}{\rho_2^3}$$

$$G_\eta = 2\eta - 2(1-m)\frac{\eta}{\rho_1^3} - 2m\frac{\eta}{\rho_2^3} \tag{4.63}$$

which follow from (4.43).

To obtain the level curves, it remains to find the initial condition to start the integration of the differential equations (4.62). This is not a trivial issue. In fact, we also do not know a priori how many disconnected components a level curve has. A study of the behaviour of G is useful.

From (4.57), observe that $G(\xi, \eta) > 0 \, \forall \xi, \eta$. Thus, for small values of the Jacobi integral, the Hill region is the whole plane. Secondly, G has two singularities in the position of the primaries $(m, 0)$ and $(m-1, 0)$. Furthermore, $G \longrightarrow +\infty$ as (ξ, η) tend to the position of the primaries or to $+\infty$. So, for large values of C, the points in a neighborhood of the primaries and the points sufficiently far away from the origin are in the Hill region, but the points in between might not.

By its definition, the Lagrangian points are points for which the partial derivatives of Ω vanish, as the conditions imposed in (4.33) to find the Lagrangian points are $\frac{\partial \Omega}{\partial \xi} = 0 = \frac{\partial \Omega}{\partial \eta}$, according to (4.26). Thus, the Lagrangian points might be a local minimum of Ω, that is, points where a component of the level curve is created; a local maximum, that is, points where a component of the level curve is destroyed or a saddle point.

According to the previous argument, it is convenient to start with the computation of the values of the Jacobi integral for which the Lagrangian points are in the 0-velocity curve. Fixed a value of the mass parameter m, it consists on imposing the 0-velocity condition (4.56) on the Lagrangian points which have been computed

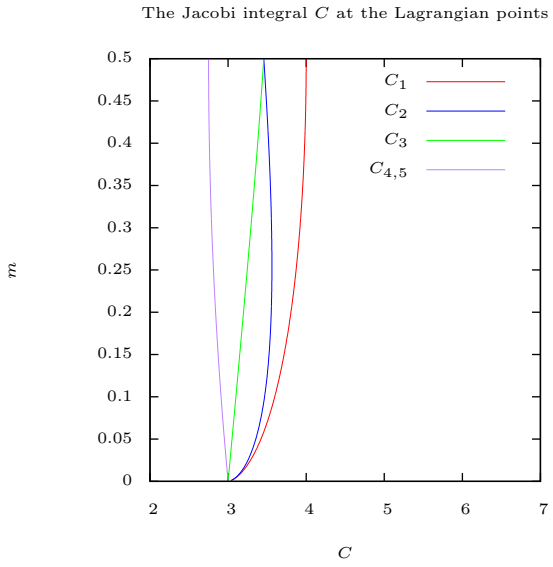

Figure 5: Values of C for which the Lagrangian points are on the 0-velocity curve.

(numerically or analytically) in Section 4.2. We denote them as $C_1, ..., C_5$. The results are summarized in Figure 4 for the value $m = 0.3$. In fact, we can obtain a simple expression of C_4 and C_5. Imposing (4.39) in (4.56), we get

$$C_4 = C_5 = 3 - m(1 - m) \tag{4.64}$$

To give some evidence that the results are similar for other values of $m \in (0, 0.5]$, we have plotted in Figure 5 the values of the Jacobi integral for which the Lagrangian equilibrium solutions are in the 0-velocity curve. The most relevant fact we can extract from it is that the order is preserved, namely

$$C_4 = C_5 \leq C_3 \leq C_2 \leq C_1 \ \ \forall m \in [0, 0.5] \tag{4.65}$$

Furthermore, as the Lagrangian equilibrium solutions are the only equilibrium solutions, the 0-velocity curves cannot change its behaviour radically for values of C different than the ones given in (4.65). Thus, we can expect that the 0-velocity curves behave, as we increase C, similarly for all the values of m.

Taking into account all these considerations, and after checking the computed results, we can sketch the evolution of the 0-velocity curves for a fixed value of mass m as the Jacobi integral C increases. See the results in Figure 6 for $m = 0.3$. To integrate the 0-velocity curves from the differential equations (4.62) we used a RKF78 (Runge-Kutta-Fehlberg of orders 7 and 8) method. See [5] for a description of the RKF45, which is analogous to RKF78 but of orders 4 and 5.

Summarizing, the behaviour of the 0-velocity curves for a fixed m, depending on C, is as follows. We indicate in parenthesis the colours corresponding to the values of C in Figure 6.

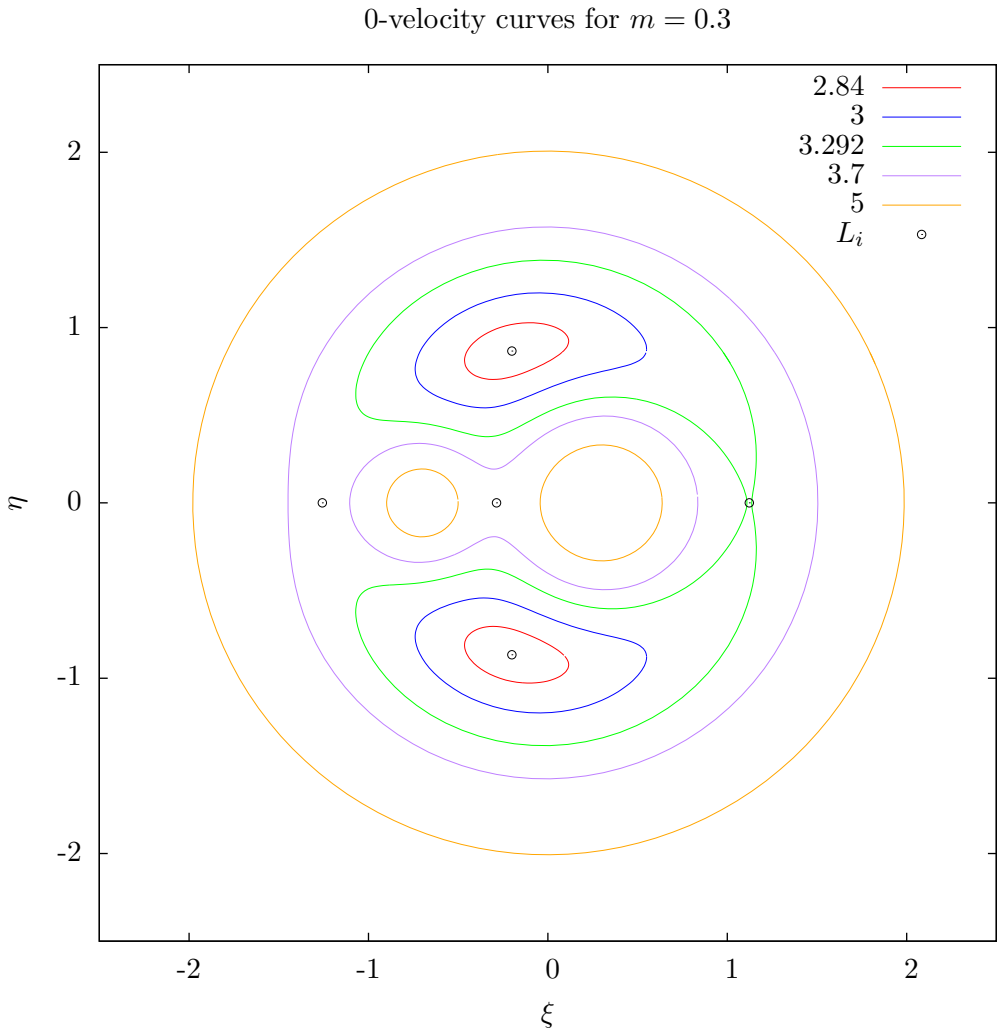

Figure 6: Lagrangian points and 0-velocity curves for different values of C, $m = 0.3$. Find the description of the Lagrangian points in Remark 4.2.

For small values of C, namely $C < C_4 = C_5$, there are no 0-velocity curves and the Hill region is the whole plane $\mathbb{R}^2$. For $C_4 < C < C_3$, two disconnected components of the 0-velocity curves appear around L_4 and L_5 (red). As C increases, the area of the two disconnected regions bounded by the 0-velocity curves also rises, similarly in the two components (blue), until they merge in a single connected region for $C = C_3$ at L_3 (green).

For $C_3 < C < C_2$, as C grows, the forbidden region continues to enclose more area, until it connects with itself at L_2 for the value $C = C_2$, giving birth to two disconnected components of Hill's region: one bounded; one unbounded. For $C_2 < C < C_1$, the area of the forbidden region continues to increase (purple), until it connects with itself in L_1 for the value $C = C_1$, when the bounded component of the Hill region divides into two bounded components. Thus, for $C > C_1$ the Hill region has 3 components: one around the first body; one around the second body; one unbounded component (orange).

4.4 Evidence of chaos

The Planar and Circular Restricted 3-Body Problem is chaotic. We would like to explore a little bit the chaos of the system. Among all the situations where chaos is appreciable and interesting, we will focus on the study of final evolutions close to parabolic orbits, for both the cases $m = 0$ and $m \neq 0$. The main objective is to find evidence of chaos and try to describe it. This will be done by finding numerical evidence of the existence of transversal homoclinic points. Throughout the section, we will try to outline the differences between the integrable Kepler's Problem ($m = 0$) and the non-integrable Planar and Circular Restricted 3-Body Problem ($m \neq 0$).

Observe that the case $m \neq 0$ can be seen as a perturbation of Kepler's Problem, for small values of m. Compare equations (3.30) and (4.12), taking into account the change of variables done in the last. This perturbation causes a big difference in the qualitative behaviour of the solutions, as we shall see. The main references followed in this section are [8], [12] and [4].

One of the main tools to study chaotic behaviour in continuous dynamical systems defined by ordinary differential equations are Poincaré maps. The description, up to what is possible, of the chaos of certain Poincaré maps associated to a continuous dynamical system gives information about the chaos in the continuous system. We recall that a sufficient condition for the existence of chaos in a discrete map is the existence of transversal homoclinic points.

Def 4.4. *Let $f : U \subseteq \mathbb{R}^n \longrightarrow \mathbb{R}^n$, $\dot{x} = f(x)$ be an autonomous ordinary differential equation (ODE), $\Sigma \subseteq U$ a codimension 1 differentiable manifold, that is, $\dim \Sigma = n - 1$. We say that Σ is transversal to the vector field f if*

$$f(x_0) \notin T_{x_0}\Sigma \quad \forall x_0 \in \Sigma \tag{4.66}$$

where $T_{x_0}\Sigma$ denotes the tangent space of Σ on x_0. The Poincaré map P defined by

Σ *is the discrete map*

$$P : \Sigma \longrightarrow \Sigma$$

such that the image of $x_0 \in \Sigma$ *is the next intersection with* Σ *of the solution of the ODE with initial condition* x_0*. In the context of Poincaré maps,* Σ *is called a Poincaré section.*

Def 4.5. *Let* (A, d) *be a metric space. A discrete map* $F : A \longrightarrow A$ *is chaotic if*

1. F *has sensitive dependence on initial conditions, that is, exists* $\epsilon > 0$ *such that*

$$\forall \delta > 0 \ \forall x \in A \ \exists y \in A \ \exists n = n(\delta) \ s.t. \ d(x, y) < \delta, \ \ d(F^n(x), F^n(y)) > \epsilon$$

2. F *is topologically transitive, that is, for all* $U, V \subset A$ *open sets there exists* $k > 0$ *such that* $f^k(U) \cap V \neq \emptyset$*.*

3. Periodic points of F *are dense in* A*.*

Def 4.6. *Consider a discrete map* $F : A \longrightarrow A$*,* q *a fixed point of* F *for which the invariant stable and unstable manifolds* W_q^s, W_q^u *exist. A point* $p \in A$ *is homoclinic if* $p \in W_q^s \cap W_q^u$*.*

Furthermore, we say that p *is transversal homoclinic if it is homoclinic and the manifolds* W_q^s, W_q^u *intersect non-tangentially in* p*.*

4.4.1 Final evolutions. McGehee coordinates

Def 4.7. *A final evolution of the Planar and Circular Restricted* 3*-Body Problem is the behaviour of an orbit of the third body as time tends to* $\pm\infty$*.*

We describe here all the possible final evolutions in this problem. As given in [8], there are four possible types of final evolutions as time tends to $+\infty$:

1) Lagrange final evolution L^+: The orbit of the third body remains bounded for all positive times.

2) Oscillatory final evolution OS^+: The distance $\rho = \rho(t)$ of the third body to the barycenter at time t satisfies

$$\limsup_{t \to +\infty} \rho(t) = +\infty; \qquad \liminf_{t \to +\infty} \rho(t) < +\infty \tag{4.67}$$

3) Parabolic final evolution P^+: The third body reaches infinity and the radial velocity $\dot{\rho}$ tends to 0 as time tends to infinity.

4) Hyperbolic final evolutions H^+: The third body reaches infinity with positive radial velocity $\dot{\rho}$.

The possible final evolutions for time $t \to -\infty$ are analogous. We denote them using the same letters, but with the superscript $^-$. If we combine all the possibilities for time tending to $+\infty$ and $-\infty$, it results in 16 possible types of final evolutions. Furthermore, it has been shown in [8] that all 16 types of final evolution can take

place for values of the mass parameter m sufficiently small (non-zero) and Jacobi integral C sufficiently large.

The role played by infinity in the classification of the orbits is fundamental, as what basically distinguishes the final evolutions of the third body is the fact of reaching infinity or not, and the way it is reached. Thus, it is convenient to introduce coordinates in which the infinity is at the origin, the so-called McGehee coordinates. McGehee coordinates (q, θ, p, ω) are defined as

$$\begin{aligned} \rho &= \frac{2}{q^2}, \qquad 0 < q < \infty \\ \dot{\rho} &= p_\rho = p \\ \omega &= p_\theta \end{aligned} \tag{4.68}$$

where $(\rho, \theta, p_\rho, p_\theta)$ denote polar synodical barycentric coordinates, as defined in Section 4.1.3. To obtain the equations in McGehee coordinates, it is convenient to take into account the similarities of the expressions of ρ_1, ρ_2 in (4.31), namely

$$\rho_1 = \frac{2}{q^2}\left[1 - mq^2\cos\theta + m^2\frac{q^4}{4}\right]^{\frac{1}{2}}; \quad \rho_2 = \frac{2}{q^2}\left[1 - (m-1)q^2\cos\theta + (m-1)^2\frac{q^4}{4}\right]^{\frac{1}{2}}$$

We shall introduce the function

$$f_\mu := \left[1 - \mu q^2\cos\theta + \mu^2\frac{q^4}{4}\right]^{\frac{1}{2}} \tag{4.69}$$

so that $\rho_1 = \frac{2}{q^2} f_m$ and $\rho_2 = \frac{2}{q^2} f_{m-1}$. The equations in McGehee coordinates are then

$$\begin{aligned} \dot{q} &= -\frac{1}{4}q^3 p \\ \dot{\theta} &= -1 + \frac{1}{4}q^4\omega \\ \dot{p} &= -\frac{1}{4}q^4 + \frac{1}{8}q^6\omega^2 + \frac{1}{4}q^4\left[1 - \frac{1-m}{f_m^3} - \frac{m}{f_{m-1}^3}\right] + \frac{m(1-m)}{8}q^6\cos\theta\left[\frac{1}{f_m^3} - \frac{1}{f_{m-1}^3}\right] \\ \dot{\omega} &= -\frac{m(1-m)}{4}q^4\sin\theta\left[\frac{1}{f_m^3} - \frac{1}{f_{m-1}^3}\right] \end{aligned} \tag{4.70}$$

Remark 4.5. *The equations of motion in McGehee coordinates are invariant under the symmetry* $(q, \theta, p, \omega, t) \mapsto (q, -\theta, -p, \omega, -t)$.

As the Hamiltonians H_1 and H_2 corresponding to Cartesian and polar barycentric coordinates coincide, the Jacobi integral is expressed in terms of McGehee coordinates as

$$C = q^2 - p^2 + 2\omega - \frac{1}{4}q^4\omega^2 + q^2\left[\frac{1-m}{f_m} + \frac{m}{f_{m-1}} - 1\right] \tag{4.71}$$

Remark 4.6. *The transformation to McGehee coordinates is not canonical.*

The parabolic orbits P^+, P^- are reinterpreted in McGehee coordinates as orbits that tend to $q = 0, p = 0$ as time t tends to $\pm\infty$. The condition $q = 0$ corresponds to reach infinity in the original coordinates while the condition $p = 0$ corresponds to 0 radial velocity. See (4.68).

Observe that the system (4.70) has a periodic orbit at $q = 0, p = 0$, as then $\dot{\omega} = 0$ and $\dot{\theta} = -1$. Thus, all variables are constant except θ, which is of the form $\theta(t) = -t + \theta_0 \in S^1$. In particular, θ is 2π-periodic in time. Furthermore, for a fixed value of C, from (4.71) we get $\omega = C/2$. We call $(q, \theta, p, \omega) = (0, \theta, 0, C/2)$ the periodic orbit at infinity. From now on, we assume that the Jacobi integral is fixed.

If the Jacobi integral C is fixed, we can eliminate the coordinate ω in a neighbourhood of $(0, \theta, 0, C/2)$: Following from (4.71), we define the function

$$g(q, \theta, p, \omega) := q^2 - p^2 + 2\omega - \frac{1}{4}q^4\omega^2 + q^2\left[\frac{1-m}{f_m} + \frac{m}{f_{m-1}} - 1\right] - C \qquad (4.72)$$

which is $\mathcal{C}^\infty$ in a neighbourhood of $(0, \theta, 0, C/2)$, $g(0, \theta, 0, C/2) = 0$ and $\frac{\partial g}{\partial \omega}(0, \theta, 0, \omega) = 2 \neq 0$ for all $\theta \in S^1$. Thus, the Implicit Function Theorem applies and there exists a $\mathcal{C}^\infty$-function $\omega^* = \omega^*(q, \theta, p)$ defined in a neighbourhood of $(0, \theta, 0)$ such that $\omega = \omega^*(q, \theta, p)$ if, and only if $g(q, \theta, p, \omega) = 0$ in a certain neighbourhood V of $(0, \theta, 0, C/2)$. To obtain the local expression $\omega = \omega^*(q, \theta, p)$ in V up to a certain order, we should do the Taylor development of ω^* around $(0, \theta, 0)$ up to the desired order

$$\omega^*(q, \theta, p) = \frac{C}{2} + \left[\frac{\partial \omega^*}{\partial q}(0, \theta, 0)q + \frac{\partial \omega^*}{\partial \theta}(0, \theta, 0)\theta + \frac{\partial \omega^*}{\partial p}(0, \theta, 0)p\right] + O_2$$

where O_2 denotes terms of order 2 or higher in q, θ and p. The required terms (successive partial derivatives of ω^* in $(0, \theta, 0)$) are obtained deriving (4.72) with respect to q, θ, p and evaluating in the point. As an illustration, for all $\theta \in S^1$, the terms up to order two are

$$\frac{\partial \omega^*}{\partial q}(0, \theta, 0) = \frac{\partial \omega^*}{\partial \theta}(0, \theta, 0) = \frac{\partial \omega^*}{\partial p}(0, \theta, 0) = 0$$

and the second order derivatives are all non-zero except

$$\frac{\partial^2 \omega^*}{\partial q^2}(0, \theta, 0) = -1; \qquad \frac{\partial^2 \omega^*}{\partial \theta^2}(0, \theta, 0) = 1$$

Thus, we obtain

$$\omega = \omega^*(q, \theta, p) = \frac{C}{2} - \frac{1}{2}q^2 + \frac{1}{2}p^2 + O_3 \qquad (4.73)$$

Further terms can be analogously obtained. We refer to [8] for a longer expression. Introducing (4.73) in (4.70), we obtain an approximation up to certain order of the equations of motion in a neighbourhood of $(0, \theta, 0, C/2)$, that is

$$\dot{q} = -\frac{1}{4}q^3 p$$

$$\dot{\theta} = -1+\frac{C}{8}q^4-\frac{1}{8}q^6+\frac{1}{8}q^4p^2+O_8 \tag{4.74}$$

$$\dot{p} = -\frac{1}{4}q^4 + \frac{C^2}{32}q^6 - \frac{C}{16}q^8 + \frac{C}{16}q^6p^2 + \frac{1}{4}q^4\left[1 - \frac{(1-m)}{f_m^3} - \frac{m}{f_{1-m}^3}\right] +$$
$$+\frac{m(1-m)}{8}q^6\cos\theta\left[\frac{1}{f_m^3} - \frac{1}{f_{m-1}^3}\right] + O_{10}$$

Again, we refer to [8] for an expression to higher orders.

We would like to describe the invariant manifolds, if they exist, of this periodic orbit. Regarding its existence, we note that the classical invariant manifold theorem for hyperbolic points, or, more generally, hyperbolic sets, does not apply, as the Jacobian matrix of the system (4.70) (and also (4.74)) at any point of the form $(0, \theta, 0, C/2)$ (resp. $(0, \theta, 0)$) for $\theta \in S^1$ is the matrix 0, and thus the periodic orbit is non-hyperbolic.

In [10], McGehee showed the existence of analytic invariant manifolds for the periodic orbit considered above. We denote the corresponding stable and unstable manifolds as W_∞^s and W_∞^u respectively, which coincide with the points with parabolic final evolution, namely

$$W_\infty^s = P^+; \qquad W_\infty^u = P^- \tag{4.75}$$

For short, we refer to them as the stable and unstable invariant manifolds at infinity.

4.4.2 The invariant manifolds W_∞^s and W_∞^u

To begin with, we describe the invariant manifolds at infinity W_∞^s, W_∞^u in the case $m = 0$. In this case, it has already been proved that a point is in P^+ if, and only if, it is in P^-. This follows from the classification of the orbits in Kepler's problem, where orbits with different final evolutions for $t \longrightarrow +\infty$ and $t \longrightarrow -\infty$ are not possible. According to (4.75), we conclude that $W_\infty^s = W_\infty^u$. Furthermore, the points in the invariant manifolds satisfy

$$H = \frac{1}{2}(p_x^2 + p_y^2) - \frac{1}{\sqrt{x^2+y^2}} = 0 \tag{4.76}$$

where H denotes the Cartesian sidereal barycentric Hamiltonian, given in (4.11), or, equivalently, the sidereal energy. We recall that for $m = 0$, the sidereal energy is a first integral. To obtain an expression of W_∞^s in McGehee coordinates, we do the corresponding changes of variables to (4.76) and obtain

$$H = \frac{1}{2}\left(p_\rho^2 + \frac{p_\theta^2}{\rho^2}\right) - \frac{1}{\rho} = \frac{p^2}{2} + \frac{\omega^2q^4}{8} - \frac{q^2}{2} = \frac{p^2}{2} + \frac{(C/2+H)^2q^4}{8} - \frac{q^2}{2} \tag{4.77}$$

where we used polar synodical barycentric coordinates as a middle step and the relation

$$C = 2(\omega - H) = 2(p_\theta - H) \tag{4.78}$$

which is interesting to outline, as it relates the Jacobi integral C, the angular momentum $p_\theta = \omega$ and the sidereal energy H.

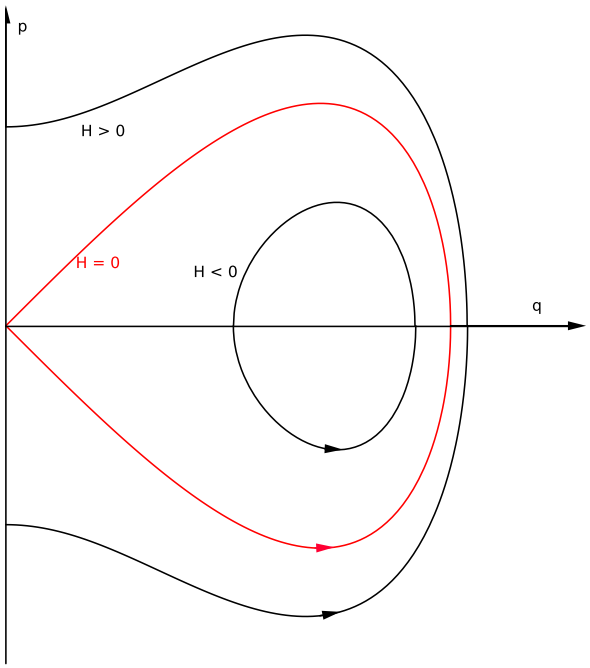

Figure 7: $m = 0, C = 4$. Energy level submanifolds in McGehee coordinates (obtained by rotating the figure around the p-axes). For $H = 0$, $W^s_\infty = W^u_\infty$ (red).

From (4.77), we get p as a function of q in the level of energy H

$$p = \pm\sqrt{q^2 - \left(\frac{C}{4} + \frac{H}{2}\right)^2 q^4 + 2H} \tag{4.79}$$

which can be plotted to obtain the different levels of energy H and thus some information about the behaviour of the orbits in McGehee coordinates. Find in Figure 7 the plot of a section at a certain angle $\theta = \theta_0$ of different levels of energy. As it can be checked by direct evaluation of the field, the flow follows the direction of the arrows indicated in the figure. Furthermore, the expression of the invariant manifolds $W^s_\infty = W^u_\infty$, that is, the parabolic orbits, is obtained imposing $H = 0$ in (4.79)

$$p = \pm\sqrt{q^2 - \frac{C^2}{16}q^4} \tag{4.80}$$

Consider now the case $m \neq 0$. The first step in the study of W^s_∞ and W^u_∞ is to find a local expression of them around the periodic orbit of infinity, that is, $(q, \theta, p, \omega) = (0, \theta, 0, C/2)$. In the previous section, we described a way to eliminate the ω-coordinate in the equations of motion in a neighbourhood of $(0, \theta, 0, C/2)$. We should consider this reduction and use here equations (4.74) instead of the more general (4.70). In [12], a local expression of W^s_∞ around the periodic orbit at infinity

is found, namely

$$p = F(q,\theta) = \sum_{j\geq 1} a_j(\theta) q^j \tag{4.81}$$

with

$$a_1(\theta) = 1, \qquad a_2(\theta) = a_4(\theta) = a_6(\theta) = a_7(\theta) = a_9(\theta) = 0, \qquad a_3(\theta) = -\frac{C^2}{2^5}$$

$$a_5(\theta) = \frac{m(1-m)}{2^5} - \frac{C^4}{2^{11}}, \qquad a_8(\theta) = \frac{9m(1-m)}{2^7}\sin(2\theta)$$

Remark 4.7. *According to the symmetry $(q,\theta,p,\omega,t) \mapsto (q,-\theta,-p,\omega,-t)$ in the McGehee equations of motion, a local expression of W^u_∞ is given by $p = -F(q,-\theta)$.*

4.4.3 The first intersection of W^s_∞ and W^u_∞ at the pericenter passage. Transversality of homoclinic points.

In this section, we find numerical evidence for the existence of transversal homoclinic points of a Poincaré map associated to McGehee equations of motion, for $m \neq 0$. This provides evidence of the chaos in the system. Furthermore, for some particular values of the parameters C and m, we will try to measure the amount of chaos. This will be done by computing a second order approximation of the angle between the invariant manifolds at a transversal homoclinic point.

Fix a value of C and consider the Poincaré section defined by the passage closest to the barycenter of the primaries, that is, a minimum of ρ. More specifically, the Poincaré section considered is

$$\Sigma := \{(q,\theta,p,\omega);\ \ p = 0,\ \text{they satisfy (4.71)}\} \tag{4.82}$$

The first objective is to describe the first intersection of W^s_∞ and W^u_∞ with the Poincaré section Σ.

For $m = 0$, imposing $H = 0$ and $p = 0$ in (4.77), we get

$$q^2\left(\frac{C^2}{16}q^2 - 1\right) = 0$$

As $q = 0$ corresponds to the periodic orbit of infinity and $q >= 0$, the intersection of $W^s_\infty = W^u_\infty$ with Σ turns out to be the circle of radius $q = 4/C$ with $\theta \in S^1$.

For $m \neq 0$, we obtain them numerically. We describe first the process for W^u_∞:

1) Obtain points close to W^u_∞ in a neighbourhood of the periodic orbit at infinity, using the expression (4.81). More specifically, choose $q > 0$ small, different values of θ equidistant in $[0, 2\pi)$ and obtain p using $p = -F(q,-\theta)$, where F is given in (4.81). Compute ω from (4.71), so that (q,θ,p,ω) is a point close to W^u_∞.

2) Simulate the orbit of the points obtained above, integrating them numerically along the McGehee field given in (4.70), until the Poincaré section Σ is crossed.

Store in memory the points before and after the crossing. We use a RKF78 method to do the numerical integration.

3) From the points obtained before and after the crossing, get a point in the Poincaré section using secant method.

The main difficulty is the choice of an adequate $q > 0$, because a decrease in q means an increase in the integration steps, which might lead to too much computing time and/or to too much error. On the other hand, an increase on q means a rise on the error in the computation of the initial point close to W^u_∞. Regarding the stable manifold W^s_∞, the process is almost the same, with the only differences that p is obtained from $p = F(q, \theta)$ and that the integration is done backwards in time.

See Figure 8 for the intersections of Σ with W^s_∞ and W^u_∞ in the case $m = 0.3$ and $C = 5.5$. We plotted there the angle θ against q. The starting values are $q = 0.04$ and $N = 350$ equidistant θ, namely $\theta_k = 2k\pi/N$ for $k = 0, \ldots, N-1$. We observe that the invariant manifolds intersect in Σ for values of θ close to 0 and π. Furthermore, this intersections seem to be transversal.

In fact, the intersections that seem close to $\theta = 0$ and $\theta = \pi$ are exactly in those values and exist for all values of C and m. This is a consequence of the symmetry $(q, \theta, p, \omega, t) \mapsto (q, -\theta, -p, \omega, -t)$, because the values 0 and π are the only values in $[0, 2\pi)$ such that $\theta_0 \equiv -\theta_0 \pmod{2\pi}$. However, other intersections might exist. See, for instance, both plots in Figure 9, where there are two more intersections of the invariant manifolds in Σ.

It is important to notice that $P^- \cap P^+ = W^u_\infty \cap W^s_\infty$. Reinterpreting it in terms of final evolutions, this shows that final evolutions of the type $P^- \cap P^+$ exist for all m and for all C. For $m = 0$, they form a two dimensional manifold that acts as a separatrix, whereas for $m \neq 0$ they contain at least two orbits (those intersecting Σ with angles $\theta = 0$ and $\theta = \pi$) and there is numerical evidence that, at least in the cases computed, it consist on a finite number of orbits and thus the separatrix is broken.

Remark 4.8. *The symmetry $(q, \theta, p, \omega, t) \mapsto (q, -\theta, -p, \omega, -t)$ also can give some idea of the error. According to it, if $(q, \theta) \in W^s_\infty \cap \Sigma$, then $(q, -\theta) \in W^u_\infty \cap \Sigma$. So, we have two ways to compute values of $W^u_\infty \cap \Sigma$, which can be compared: direct integration from a point in W^u_∞ as previously described or integrating a point in W^s_∞ an applying the symmetry once Σ is reached.*

It remains to discuss the transversality of the homoclinic points already found. To that end, we will find an approximation of the curves plotted in Figure 8, that is, $W^s_\infty \cap \Sigma$ and $W^u_\infty \cap \Sigma$ in McGehee coordinates. Call the function we want to approximate h. We apply a discrete Fourier transform, as h is 2π-periodic and we only know its value in a finite number of points.

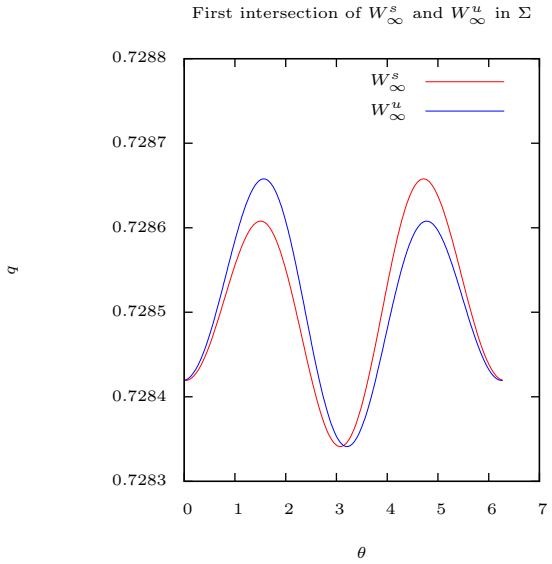

Figure 8: $m = 0.3$, $C = 5.5$. The first intersection of the invariant manifolds W^s_∞ and W^u_∞ with the Poincaré section Σ.

Discrete Fourier Transform (DFT)

Consider the finite vector space E_n generated by $\{\psi_0, \ldots, \psi_{2n}\}$ with the usual vector sum and scalar multiplication, where

$$\psi_0(\theta) := \frac{1}{2}; \qquad \psi_{2k-1} := \cos(k\theta); \qquad \psi_{2k} := \sin(k\theta) \tag{4.83}$$

for $k = 1, \ldots, n$. Consider $n+1$ equidistant points in $[0, 2\pi]$, namely

$$\theta_k = \frac{2\pi k}{n+1} \qquad \text{for } k = 0, 1, \ldots, n \tag{4.84}$$

and define the scalar product $\langle \cdot, \cdot \rangle_n$ in E_n by

$$\langle g_1, g_2 \rangle_n := \sum_{j=0}^{n} g_1(\theta_j) g_2(\theta_j) \qquad \forall g_1, g_2 \in E_n \tag{4.85}$$

It can be checked that the generators $\{\psi_0, \ldots, \psi_{2n}\}$ are orthogonal. Furthermore,

$$\langle \psi_i, \psi_j \rangle_n = \begin{cases} 0 & \text{if} \quad i \neq j \\ \frac{n+1}{4} & \text{if} \quad i = j = 0 \\ \frac{n+1}{2} & \text{if} \quad i = j > 0 \end{cases} \tag{4.86}$$

According to the orthogonal projection theorem, h_n is the best approximation of h in E_n if, and only if

$$\langle h - h_n, g \rangle_n = 0 \qquad \forall g \in E_n \tag{4.87}$$

Due to the orthogonality of the generators, the normal equations are diagonal, so the coefficients of the solution

$$h_n(\theta) := a_0\frac{1}{2} + \sum_{j=1}^{n} a_j \cos(j\theta) + \sum_{j=1}^{n} b_j \sin(j\theta) \tag{4.88}$$

are given by

$$\begin{aligned} a_0 &= \frac{\langle \psi_0, h\rangle_n}{\langle \psi_0, \psi_0\rangle_n} = \frac{2}{n+1}\sum_{k=0}^{n} h(\theta_k) \\ a_j &= \frac{\langle \psi_{2j-1}, h\rangle_n}{\langle \psi_{2j-1}, \psi_{2j-1}\rangle_n} = \frac{2}{n+1}\sum_{k=0}^{n} h(\theta_k)\cos(j\theta_k) \\ b_j &= \frac{\langle \psi_{2j}, h\rangle_n}{\langle \psi_{2j}, \psi_{2j}\rangle_n} = \frac{2}{n+1}\sum_{k=0}^{n} h(\theta_k)\sin(j\theta_k) \end{aligned} \tag{4.89}$$

for $j = 1, \ldots, n$. See [3] or [5] for more details.

After the numerical integration, the angles obtained are not equidistant. To find the discrete Fourier transform we need equidistant angles θ_k. To obtain them, it is needed to interpolate the pairs (q, θ). We have used a Lagrange interpolation method with 6 interpolation points. Furthermore, one can obtain more values using this interpolation, which are much faster to compute than the numerical integration described above. In the next computations, we will double the number of points in Σ with this strategy.

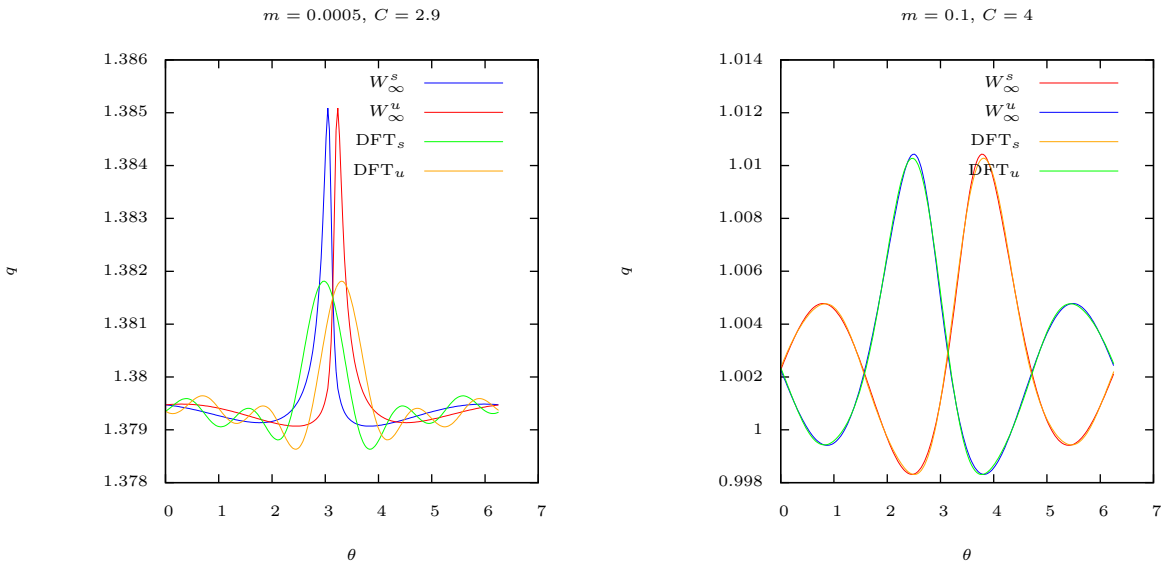

Figure 9: Samples of discrete Fourier transform for different values of m and C. We denote DFT_s for W^s_∞ and DFT_u for W^u_∞.

See some examples of the discrete Fourier transforms obtained in Figure 9. Here we used $q = 0.08$ and $N = 100$ as starting values, to reduce the computing time of the

numerical integration. The Fourier expansions have been computed up to order 6. First of all, we observe that the approximation on the left is not accurate enough, specially around π. More Fourier terms and/or more points in the intersection of the invariant manifolds at Σ would have been needed. This is a consequence of the sharp form the function has. See a possible explanation at the end of this section. On the other hand, the computations on the right have smaller error.

Remark 4.9. *Other computations of $W^u_\infty \cap \Sigma$ and $W^s_\infty \cap \Sigma$ with higher values of C have also been done, but as the splitting of the manifolds becomes almost imperceptible, the plots have not been included. Furthermore, the computations of the DFT have also been done for the values in Figure 8, but as the differences were not appreciable in the plot, we do not plot them.*

From the obtained Fourier expressions, one can compute the approximate slope of the functions corresponding to W^u_∞, W^s_∞, at the intersection points. The derivative of $h_n(\theta)$ is

$$\frac{dh_n}{d\theta} = \sum_{j=1}^{n} j b_j \cos(j\theta) - \sum_{j=1}^{n} j a_j \sin(j\theta) \tag{4.90}$$

Direct evaluation of the derivative with the computed Fourier coefficients at the homoclinic tangency corresponding to $\theta = \pi$, show that the slopes for the case $m = 0.1, C = 4$ (the right part of Figure 9) are

$$W^s_\infty : 1.4658 \times 10^{-2}; \qquad W^u_\infty : -1.4658 \times 10^{-2} \tag{4.91}$$

The slope corresponds to the tangent of the angle with respect to the horizontal line. As the Taylor development of the tangent function around 0 is $\tan x = x + O_3(x)$, the angle between the manifolds is approximated at second order by $\alpha = 2.9316 \times 10^{-2}$. This gives numerical evidence, in this particular case, of the existence of a transversal homoclinic point, as it was expected from the plots. As the computations have been done without using the symmetry described in Remark 4.8, the fact that the slopes are almost the same after changing signs gives consistency: If $W^s_\infty \cap \Sigma$ is described by a function of the form $q = h(\theta)$, then $W^u_\infty \cap \Sigma$ is described by $q = h(-\theta)$. Thus, its derivatives are $h'(\theta)$ and $-h'(-\theta)$.

Remark 4.10. *In order to proof rigorously that the tangency is transversal, this process could be repeated bounding the errors at every step we have done, that is: approximation at the invariant manifold, numerical integration, secant method, interpolation and discrete Fourier transform, with the hope to conclude that the slopes cannot coincide. Let me be quite pessimistic on the effectiveness of this method, as there are many steps to be done that increase the error, specially those in the numerical integration, and the slopes are relatively close, being the difference of order 10^{-2}.*

Another way to try to measure the chaos of the system could be to measure the maximal splitting of the manifolds. For instance, in Figure 8, it is less than 10^{-4} and in the right part of Figure 9 is approximately 1.2×10^{-2}.

Taking into account what has been said in this section, it seems reasonable to conjecture that for large C, the intersections of Σ with the invariant manifolds W^u_∞ and W^s_∞ are very similar, and thus the splitting very small. However, they do intersect in Σ non-tangentially. In fact, in [8] it is proved that for sufficiently large C and sufficiently small m, W^u_∞ and W^s_∞ intersect Σ in two curves analytically diffeomorphic to circles. Furthermore, the intersection $W^u_\infty \cap W^s_\infty$ is non-tangential at $\theta = 0$ and $\theta = \pi$, and thus, the existence of at least two homoclinic points is proved.

But, for small C, specially when $C < C_2$, the Hill region has only one connected component, and thus the third body could eventually get close to the primaries, increasing strikingly the amount of chaos present in the system. So, one has to be cautious on the results of the left plot in Figure 9, as there might exist initial values in which the third body gets really close to the primaries, with much bigger values of q that those found to do the plot, and thus make the plot differ considerably from reality. This is supported by the fact that, for $C = 2.9$ and $m = 0.0005$, we have

$$C = 2.9 < C_4 = C_5 < C_2$$

according to (4.64). Thus, the Hill region is the whole plane $\mathbb{R}^2$, so the third body could eventually get really close to the primaries. We have not found numerical evidence apart of the sharp form of the function in the left hand side of Figure 9, but it is something that can not be discarded.

4.4.4 Further intersections of W^s_∞ and W^u_∞ at the pericenter passage.

Once the first intersection of the invariant manifolds W^s_∞ and W^u_∞ with the Poincaré section Σ has been described, we would like to describe further intersections. Somehow, this is an attempt to get closer to an Oscillatory solution and to describe the chaos in the system originated by final evolutions. In [8] it is proved that for sufficiently large C and sufficiently small m, W^u_∞ and W^s_∞ intersect Σ in two curves analytically diffeomorphic to circles. Furthermore, W^s_∞ and W^u_∞ are diffeomorphic to cylinders. We restrict to this case for the rest of this section.

See Figure 10 for a representation of the situation taken into account, in Cartesian coordinates. In the representation, the splitting has been exaggerated, as for those values of the parameters m and C it is almost imperceptible in Cartesian coordinates. As W^s_∞ is diffeomorphic to a cylinder in a three dimension manifold (once C has been fixed), for increasing times, the orbits that intersect Σ inside the curve defined by $W^s_\infty \cap \Sigma$ will return to the Poincaré section, whereas the orbits that intersect Σ outside this curve will escape. The same is valid for the curve defined by $W^u_\infty \cap \Sigma$, but for decreasing time. We note that oscillatory orbits, for instance OS^+, intersect Σ infinitely many times as $t \longrightarrow +\infty$ inside the curve defined by P^+.

We focus now on obtaining the second intersection of W^u_∞ with Σ. We could do analogous arguments for W^s_∞. According to what has been previously discussed, the orbits in W^u_∞ that will return to Σ are those that cut Σ inside the curve defined

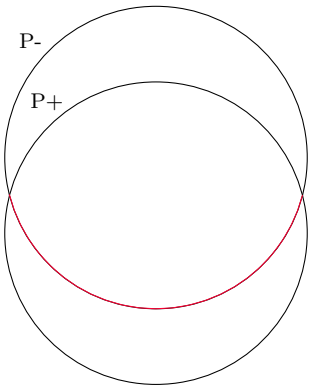

Figure 10: Representation of the first intersections of $W^s_\infty = P^+$ and $W^u_\infty = P^-$ in Σ, for large enough C and small enough m. In red, the orbits in W^u_∞ that return a second time to Σ.

by $W^s_\infty \cap \Sigma$. In Figure 10, these orbits are marked in red.

We have tried to continue the integration of the orbits in W^u_∞ that we know that will return to Σ. With the personal computer in hand, this does not work, as it requires too much computing time to make the passage close to the periodic orbit at infinity ($q = 0, p = 0$). In fact, this passage has not been achieved by any of the initial conditions tried. An explanation of this could be that the first term in the McGehee field corresponding to the variable p is of order 4 in p and q. Thus, at a passage close to $p = 0$, $q = 0$ the field is really small, so the integration steps done by the RKF78 are tiny, of the order of hq^4 (see (4.70)), where h is the step size used in the numerical integration.

5 Conclusions

It comes now the time to recapitulate and evaluate what we have done in this thesis.

1. Kepler's Problem and the 2-Body Problem have been revised, as they are the logical first step in the study of the 3-Body Problem and play an important role in the Planar and Circular Restricted 3-Body Problem (PCR3BP). On the one hand, the PCR3BP can be seen as a perturbation of Kepler's Problem for small values of the mass parameter m. On the other hand, in any Restricted 3-Body Problem, the primaries behave as in the 2-Body Problem.

   However, the solution to Kepler's problem has not been completely determined, in the sense that it depends on the computation of some integrals. What has been done is a complete classification of the trajectories of the body in terms of the Energy E, and some intuition on how it moves has been given by $L = r^2\dot{\varphi}$, see (3.17), where the angular momentum L is constant in time. In particular, this completely determines the motion in the circular case, as then the angular velocity is constant. As the 2-Body Problem has been reduced to Kepler's Problem, the same is valid for it.

2. The Planar and Circular Restricted Three-Body Problem has been presented. The Lagrangian equilibrium solutions and their stability have been studied. The first integral of the system, the Jacobi integral C has been introduced and used to determine the Hill regions depending on it. Numerical methods have been used to compute the collinear Lagrangian equilibrium for several values of m and the boundary of the Hill region for a fixed value of m and several values of C. Arguments have been given to justify that the behaviour is similar for other values of m.

3. Numerical evidence of chaos for some values of m and C has been provided through evidence of the existence of transversal homoclinic points of the Poincaré map associated to the Poincaré section Σ. This has been done by computing the first intersection of W^u_∞ and W^s_∞ with Σ, and computing an approximation of the intersection curves using a discrete Fourier transform.

4. In order to describe the chaos arising from the previous transversal homoclinic points, we have tried to compute the further intersections of W^u_∞ and W^s_∞ with Σ by continuing the numerical integration, although not successfully. An argument on why this might happen has been provided.

5. Several numerical methods such as Newton method, secant method, Lagrange interpolation, discrete Fourier transform, Davidenko method and RKF78 have been used. The first four were already known to me at the beginning of the project, but the other two were not. Having dealt with all of them is also an important part of this thesis.

Further work related to this thesis could be:

1. Look for another way than the described in conclusion 4. to deal with the successive cuts of W^u_∞ and W^s_∞ with Σ. A possibility is to build a model for the Poincaré map, as described in [4] and [12]. There, the return maps are approximated by standard-like maps in suitable domains.

2. Do a qualitative study of the successive cuts of W^u_∞ and W^s_∞ with Σ. This turns out to be successful, as seen in [4].

3. Explore other aspects of the problem, such as passages close to the primaries. This is also another source of chaos. This would be particularly useful in the study of hypothetic collisions.

4. Improve some of the numerical algorithms used. For instance, the Fast Fourier Transform (FFT) algorithm to compute the discrete Fourier transform has not been used or try to use a Newton method to substitute the secant method in the approach to the Poincaré section Σ. However, the big computing requirements are due to the long numerical integration, so not much will be improved in this particular case, although it is something worth learning.

I would like to conclude saying that this thesis has been a challenge. I have learned a lot from having to look for sources, reading some research articles and the mere fact of writing this report. I have experienced how difficult is to write a text in mathematics. Also, this thesis has developed on me new interests, such as discrete maps, as they play a fundamental role in the description of chaos in continuous dynamical systems.

References

[1] Abraham, R. and Marsden, J., *Foundations of Mechanics*. Benjamin/Cummings, 1978.

[2] Arnold, V.I., *Mathematical Methods of Classical Mechanics*. Springer-Verlag, 1978.

[3] Aubanell, A., Benseny, A. and Delshams, A., *Eines bàsiques de càlcul numèric : amb 87 problemes resolts*. Bellaterra : Publicacions de la Universitat Autònoma de Barcelona, 1991.

[4] Benseny, A., *Contribució a l'estudi del problema restringit de* 3 *cossos per a valors petits del paràmetre de masses*. 1984.

[5] Burden, R.L. and Faires, J.D., *Numerical Analysis*. International Thompson, 2002.

[6] Celletti, A., *Stability and Chaos in Celestial Mechanics*. Springer-Verlag, 2011.

[7] Devaney, R.L., *An Introduction to Chaotic Dynamical Systems. Second Edition*. Westview Press, 2003.

[8] Llibre, J. and Simó, C., *Oscillatory Solutions in the Planar Restricted Three-Body Problem*. Mathematische Annalen, vol. 248 no. 2, pp.153-184, 1980.

[9] Masoliver, J., *Fonaments de física: Grau de matemàtiques*. Barcelona: Publicacions de la Universitat de Barcelona, 2010.

[10] McGehee, R. *A stable manifold theorem for degenerate fixed points with applications to Celestial Mechanics*. J. Differential Equations, vol. 14, pp. 70-88, 1973.

[11] Meyer, K.R. and Hall, G.R., *Introduction to Hamiltonian Dynamical Systems and the N-Body Problem*. Springer, 1992.

[12] Martínez, R. and Simó, C., *The invariant manifolds at infinity of the RTBP and the boundaries of bounded motion*. Regular and Chaotic Dynamics, vol. 19 no. 6, 2014.

[13] Szebehely, V.G., *Theory of Orbits*. New York: Acad. Press, 1967.

[14] Valtonen, M.J. and Karttunen, H., *The Three-Body Problem*. Cambridge University Press, 2006.